

JPL Document D-65830

TECHNOLOGY DEVELOPMENT FOR EXOPLANET MISSIONS

Technology Milestone Whitepaper

Phase-Induced Amplitude Apodization Corona- graph: Monochromatic Contrast Demonstration

Olivier Guyon, PI

Glenn Schneider, Laird Close, Brian Kern, Andreas Kuhnert, Amir Giveon, Laurent Pueyo, Stuart Shaklan, Ruslan Belikov, Eugene Pluzhnik, Frantz Martinache, Thomas Greene, Kerri Cahoy, Robert Vanderbei, Jeremy Kasdin, Stephen Ridgway, Domenick Tenerelli, Robert Woodruff, Alan Duncan, Tony Hull

10 August 2010

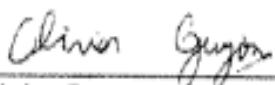
National Aeronautics and Space Administration

Jet Propulsion Laboratory
California Institute of Technology

Copyright 2011. All rights reserved.

Approvals

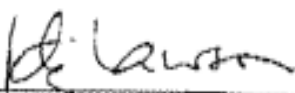
Released by



Olivier Guyon,
Principal Investigator

JUNE 07, 2010

Approved by



Peter R. Lawson,
Exoplanet Program Technology Investigation Manager, JPL

6/21/2010



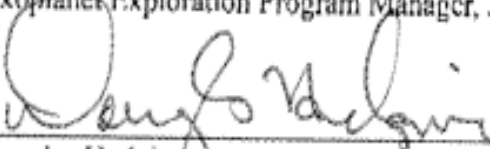
Mark Levine,
Exoplanet Exploration Technology Facilities Manager, JPL

6/21/2010



Michael Devirian
Exoplanet Exploration Program Manager, JPL

6/23/10



Douglas Hudgins
Exoplanet Exploration Program Scientist, NASA HQ

8/25/10



Lia LaPiana
Exoplanet Exploration Program Executive, NASA HQ

6/23/10

TABLE OF CONTENTS

1. Objective.....	1
2. Introduction.....	1
2.1. Phase-Induced Amplitude Apodization	1
2.2. Current status of PIAA coronagraph technology	3
2.3. PIAA mirrors: requirements and possible limiting factors	4
2.4. The Pupil mapping Exoplanet Coronagraphic Observer (PECO).....	6
2.5. Coronagraph requirements for flight mission	6
3. Milestone description: PIAA Monochromatic Contrast Demonstration	9
3.1. Milestone definition	9
3.2. Description of PIAA laboratory configuration	10
3.3. Differences between Laboratory Demonstration and Flight.....	11
4. Computation of the Metric.....	12
4.1. Definitions.....	12
4.2. Measurement of the Star Brightness	15
4.3. Measurement of the focal plane scale	15
4.4. Measurement of the Coronagraph Contrast Field	16
4.5. Contrast value for a single measurement	16
4.6. Milestone Validation Demonstration Procedure.....	18
5. Success Criteria.....	19
6. Certification Process	19
6.1 Milestone Certification Data Package.....	20
7. References.....	20
Appendix A: PIAA coronagraph architecture.....	23
Appendix B: Possible future milestones and relationship between testbeds	30
Appendix C: Pointing control	32
Appendix D: Inverse PIAA optics	35

1. Objective

In support of NASA's Exoplanet Exploration Program and the ROSES Technology Development for Exoplanet Missions (TDEM), this whitepaper explains the purpose of the first TDEM Milestone for Phase-Induced Amplitude Apodization Coronagraphy (monochromatic contrast demonstration), specifies the methodology for computing the milestone metric, and establishes the success criteria against which the milestone will be evaluated.

The TDEM PIAA proposal describes two milestones:

- Milestone 1: reaching 10^{-9} contrast at $2 \lambda/D$ in monochromatic light
 - Milestone 2: polychromatic light test, with no commitment to contrast level, but with analysis of the lab results to identify the major contributions to residual light in the high contrast area
- The current whitepaper is describing milestone 1 only, with the expectation that milestone 2 will be formulated upon completion of milestone 1.

2. Introduction

The Technology Milestones serve to gauge the developmental progress of technology for a space-based mission, such as PECO [1-5], that would detect and characterize exoplanets, and the mission's readiness to proceed from pre-Phase A to Phase A. Completion of the milestones is to be documented in a report by the Principal Investigator and reviewed by NASA HQ.

Our milestone #1 addresses narrowband starlight suppression at small inner working angles with a PIAA coronagraph, a high-efficiency coronagraphy technique enabling high-contrast imaging at a small inner working angle ($2 \lambda/D$ for the configuration to be tested) [6-15]. The approach for accomplishing the milestone is similar to the one implemented for TPF-C Milestone #1, which demonstrated narrow band starlight suppression on the High Contrast Imaging Testbed (HCIT). For this milestone a new approach, significantly different than proposed for TPF-C starlight suppression, is to be demonstrated by experiments in HCIT using an optical breadboard, wavefront control, and data processing algorithms. The demonstration will be performed on a new optical table, with appropriate changes in coronagraph configuration, light sources, and algorithms to adapt the HCIT to these series of starlight suppression experiments. A future milestone, not described in this document, will address starlight suppression with an upgraded breadboard featuring a flight-like PIAA optical configuration to be tested in polychromatic light.

2.1. Phase-Induced Amplitude Apodization

PIAA is a lossless beam apodization technique. PIAA coronagraph architectures are discussed in Appendix A, and we briefly summarize the technique in this section. Beam apodization is very useful in coronagraphy: an apodized pupil produces a high contrast image free of Airy ring. The conventional method to apodize the pupil is to introduce in the beam a mask which is fully transmissive in the center and becomes opaque at the edge of the pupil. With PIAA, the same apodized pupil is created by geometric redistribution of the light rather than selective absorption. This is achieved by aspheric optics (mirrors or lenses), as illustrated in Figure 1.

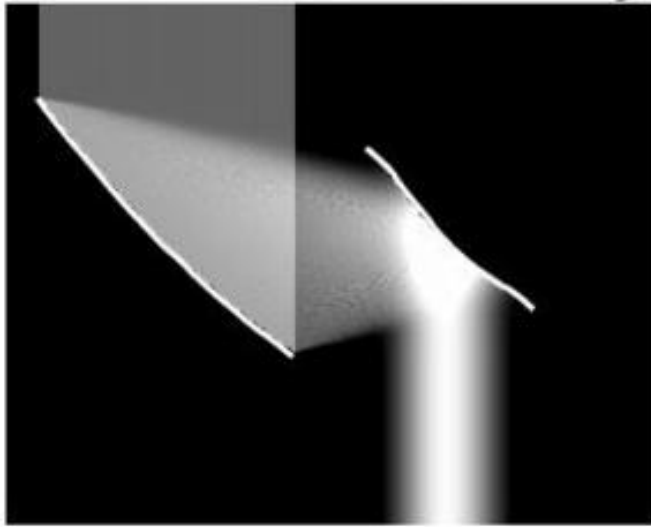


Figure 1: PIAA uses aspheric optics to apodize a beam.

The Airy rings produced with a conventional imaging telescope are due to diffraction originating from the sharp edges of the pupil. Pupil apodization, by creating a soft-edged pupil, can therefore greatly reduce these rings, and can be used either by itself or in combination with other coronagraph techniques (for example, the apodized pupil Lyot coronagraph which combines pupil apodization with Lyot coronagraphy). The conventional technique used to apodize the telescope beam is with an amplitude mask (continuous or binary) with variable transmission from the center to the edge of the pupil. This leads to a difficult compromise between reaching high contrast (which requires a strong apodization) and achieving high coronagraph throughput &

good angular resolution (which both favor a weak apodization). In a conventional apodized pupil coronagraph, for example, reaching 10^{-10} contrast requires a strong apodization with a 10% throughput which degrades the telescope's angular resolution to approximately $2.5 \lambda/D$ (instead of $1 \lambda/D$) and does not allow high contrast imaging within approximately $4 \lambda/D$.

With PIAA optics, strong apodizations can be achieved with no loss in throughput or angular resolution, enabling high contrast imaging at small angular separation from the optical axis with almost no loss in efficiency. The PIAA's inner working angle at high contrast ranges from $0.64 \lambda/D$ for an aggressive PIAA design to $2 \lambda/D$ for a more conventional PIAA design (design choice depends on the goal contrast, manufacturing capabilities, ability to mitigate chromatic issues and angular size of the central source). PIAA does not absorb light, and it therefore preserves the sensitivity and angular resolution of the telescope. When implemented with mirrors, PIAA can be made to operate at high contrast over a wide spectral band.

The performance gain offered by PIAA for detection and characterization of exoplanets over other coronagraph is quantified in [13]. Compared to the more conventional coronagraphs which were considered for TPF-C, adopting the PIAA is equivalent to a 2x to 3x gain in telescope diameter. Recent improvements on the PIAA concept may allow even higher performance, with high contrast detection of exoplanets closer in than $2 \lambda/D$ [15].

Direct imaging and characterization of potentially habitable exoplanets with a PIAA coronagraph is therefore possible with a medium-size space telescope at optical wavelength. This was explored by two of the NASA-funded medium class Astrophysics Strategic Missions Concept Studies (PECO and ACCESS). PIAA is also a candidate for a smaller mission (the EXCEDE 0.5-m diameter mission concept [16]) and for the larger ~ 4 -m diameter Terrestrial Planet Finder Coronagraph mission [17]. The potential of the PIAA is now widely recognized. The realization of PIAA in future missions awaits proof of technical readiness traceable to space-based exoplanet mission science requirements and implementation constraints.

2.2. Current status of PIAA coronagraph technology

PIAA technologies have been developed through laboratory demonstrations and modeling since late 2002. A PIAA coronagraph testbed effort was initiated at Subaru Telescope / Research Corporation of the University of Hawaii. This monochromatic testbed in air includes reflective PIAA optics, a 32x32 MEMS deformable mirror for wavefront control, and a coronagraphic low order wavefront sensor (CLOWFS) for accurate pointing/focus measurement. This testbed demonstrated 2×10^{-7} raw contrast in monochromatic light at $1.65 \lambda/D$ separation in air [18] and a $10^{-3} \lambda/D$ closed loop pointing control [19], corresponding to 0.1 mas on PECO. Raw contrast performance was limited by incoherent ghosts in the system, which used several lenses without anti-reflection coatings. The testbed however demonstrated control of static coherent light at the 3.5×10^{-9} contrast level: over a few hours of testbed operation, the time-averaged complex amplitude in the focal plane corresponds to a 3.5×10^{-9} contrast. The Subaru testbed effort was discontinued in early 2009 and its final results have been compiled in a publication [18].

A new testbed effort dedicated to PIAA technology development was initiated at NASA Ames in 2008. The non-vacuum testbed, optimized to provide flexibility and rapid testing of new configurations/components, operates in air and has recently reached raw contrasts of 10^{-7} at $2 \lambda/D$ with a lens-based PIAA system [20]. While ongoing calibration and environment stabilization upgrades will likely augment this testbed's raw contrast performance to 10^{-8} or better, a vacuum testbed is required to meet flight mission contrast requirements.

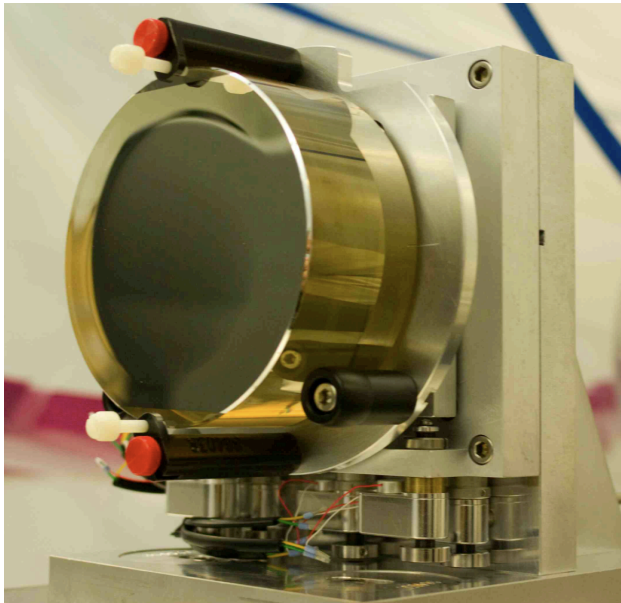


Figure 2: Zerodur PIAA M1 fabricated by Tinsley. The mirror substrate size is 120 mm diameter, while the clear aperture is 90 mm diameter. The rapid change in radius of curvature at the edge of the clear aperture is visible in this picture, and is the most challenging feature of the mirror for manufacturing, testing and alignment. This mirror is currently undergoing ion beam figuring to compensate for a figure error due to a misalignment during optical testing.

The vacuum high contrast imaging testbed (HCIT) at NASA JPL has been testing the PIAA coronagraphs since March 2009. A description of the PIAA testbed and early results are documented in Kern et al. 2009 [21]. The tests at HCIT have been performed using two prototype sets of PIAA mirrors:

- Set 1: PIAA mirrors fabricated by Axsys Imaging Technologies under contract with NOAO (funded by a NASA JPL grant for development of technologies for TPF), and delivered in mid 2006. These nickel-plated aluminum mirrors are suitable for monochromatic work, but their design is not suitable for contrast in broadband light (contrast limited to 10^{-7} in a 20% wide band with perfect optics but no wavefront correction). At the time the mirrors were designed, chromatic effects due to diffractive propagation through the PIAA system were not understood, and compensation of chromatic errors through mirror shape design was not implemented. These mirrors are currently under testing at HCIT, and a 4×10^{-7} contrast has been so far achieved in a 2 to 4 λ/D dark zone (late Feb 2010).
- Set 2: PIAA mirrors fabricated by Tinsley/L-3 under contract with NASA Ames, and delivered in April 2009. One of the mirrors in this set is shown in Figure 2. This set of Zerodur mirrors was designed to deliver 10^{-10} contrast in a 20% wide band in the absence of wavefront or coating errors, using a design optimization scheme which takes into account chromatic effects due to diffractive propagation between the mirrors. In the first 2-month long PIAA test run at HCIT a 4×10^{-7} contrast was reached at 2.5 λ/D . These preliminary tests exposed an unexpected system wavefront error which was not in agreement with the surface figure measurements performed at Tinsley. The mirrors were sent back to Tinsley to investigate this issue. The wavefront error has been found to be due to an error in the positioning of the computer generated hologram (CGH) during PIAA mirror optical testing at Tinsley. The mirrors had therefore been polished to the wrong prescription, with a 300nm peak departure from the ideal shape. The source of this problem has been confirmed by Tinsley by re-analysis of the CGH alignment procedure and independent profilometry measurements of the mirrors shapes. Tinsley is currently (April 2010) working under contract with NASA Ames Research Center to refigure the mirrors to the original prescriptions with narrow-beam ion beam figuring [22], with delivery of the mirrors scheduled for summer 2010.

The milestone described in this whitepaper is currently planned around the Axsys PIAA mirrors, as they are suitable for high contrast in monochromatic light. The surface quality of the Tinsley and Axsys mirrors are sufficient for the Milestone #1 experiment; in each case the mirrors are unlikely to be a limiting factor in the experiment. We may decide to shift to the Tinsley mirrors before completing the milestone, depending on the success of the optical refiguring, as their higher optical quality will facilitate high contrast work even in monochromatic light. Future milestones in polychromatic light will require using the Tinsley/L-3 PIAA mirrors; in broadband experiments, beyond the scope of Milestone #1, the current 300-nm surface-figure error of the Tinsley mirror-set would be a limiting factor.

2.3. PIAA mirrors: requirements and possible limiting factors

Mirrors surface figure: The highly aspheric shape of the PIAA mirrors makes them challenging to manufacture to high surface accuracy. Mirror surface errors can however be corrected by the system's deformable mirror, provided that the errors are within the range of motion of the actuators. The figure errors on Axsys mirrors currently in use in the HCIT are well within the deformable mirror's range, and we therefore do not expect the mirror surface errors to be a limiting factor for this milestone. We note that high contrast imaging in polychromatic light does require

higher wavefront quality on the mirrors, as surface errors can, through chromatic diffractive propagation, introduce errors which the deformable mirrors cannot fully remove.

Reflectivity uniformity: Reflectivity variations across the beam are not expected to be a serious issue in monochromatic light (milestone #1) as long as they are not excessive (in which case the DM stroke would be insufficient to compensate them), and can be fully compensated with a single DM over the dark zone geometry proposed. In polychromatic light (future milestone), reflectivity variations require two DMs to be efficiently corrected. While we recognize the importance of reflectivity variation for future milestones, we do not plan to investigate this issue during our milestone 1 activity, as it is not expected to be on the critical path to achieving the milestone described in this document.

Polarization effects: Reflection on the aspheric PIAA mirror surfaces will introduce some polarization variations across the beam. Breckinridge & Oppenheimer 2004 [23] point out that this effect can be problematic in high contrast imaging systems. The loss of contrast due to polarization effects is a known issue affecting all coronagraphs, and will be studied as part of the overall error budget and modeling effort. For this milestone, polarization will be studied and addressed only to the extent that it limits the achievable contrast above the contrast value specified for the milestone.

We note that in a flight system, the strongest polarization effects originate from the telescope (primary mirror and secondary mirror), not the PIAA optics, as the variation in angle of incidence on PIAA (2 deg amplitude for a F/10 PIAA system) are milder than on the telescope primary mirror (26 deg for an F/2 primary mirror, 14 deg for an F/4 primary mirror): the Axsys and Tinsley PIAA system are at F/15 and F/10 respectively, while the telescope primary mirror is faster. We therefore realize that demonstration of 10^{-9} contrast in HCIT would not be sufficient to justify that polarization is a non-issue, and modeling will be required to address this problem. Previous work on this subject has been done, with close attention to coating properties [24], and suggests that polarization issues can be mitigated through coating design to achieve 10^{-10} contrast in broadband light. This work was however done for a different telescope system (8 x 3.5 m primary mirror, with a 12 deg maximum angle of incidence) with a different coronagraph concept which did not attempt to reach $IWA = 2 \lambda/D$ (since most of the polarization error is introduced at low spatial frequency, this may be a more serious issue for PIAA). We note that PECO calls for two polarimetric channels, which mitigates this issue, especially if the orientation of the channels is properly chosen. We recognize that this issue will need to be revisited, and may lead to a modification in the coating design for the primary mirror or a change in the telescope optical design. We however do not plan to devote PIAA TDEM resources to this study as part of our milestone 1 work, unless we identify that this is limiting performance. We note that previous work on HCIT with non-PIAA coronagraphs but with similar variations in the angle of incidence across the beam achieved better than 10^{-9} contrast, and we therefore do not expect polarization effects due to variations in the angle of incidence on optics to prevent us from reaching 10^{-9} contrast. We also note, as stated in 5.1. under Success Criteria, that for this milestone, we do not require the 10^{-9} contrast to be reached in dual polarization.

2.4. The Pupil mapping Exoplanet Coronagraphic Observer (PECO)

The Pupil-mapping Exoplanet Coronagraphic Observer (PECO) mission concept uses a coronagraphic 1.4-m space-based telescope to both image and characterize extra-solar planetary systems at optical wavelengths. Figure 3 shows the PECO spacecraft and telescope assembly. PECO can detect 10^{-10} contrast sources at $2 \lambda/D$ separation (0.15") using a high-performance Phase-Induced Amplitude Apodization (PIAA) coronagraph which remaps the telescope pupil and uses nearly all of the light coming into the aperture. For exoplanet characterization, PECO acquires narrow field images simultaneously in 16 spectral bands over wavelengths from 0.4 to 0.9 μm , utilizing all available photons for maximum wavefront sensing and sensitivity for imaging and spectroscopy. The optical design, shown in Figure 4, is optimized for simultaneous low-resolution spectral characterization of both planets and dust disks using a moderate-sized telescope. PECO will image the habitable zones of about 20 known F, G, K stars at a spectral resolution of $R \sim 15$ with sensitivity sufficient to detect and characterize Earth-like planets and to map dust disks to within a fraction of our own zodiacal dust cloud brightness.

A broad overview of the PECO mission can be found in the PECO team's report to astro2010 [2], available on http://caao.as.arizona.edu/PECO/PECO_Report.pdf.

Detailed information on the PECO mission can be found in the following documents:

- The PECO Science Requirements Document [3] available on:
http://caao.as.arizona.edu/PECO/PECO_SRD.pdf
- The PECO Design Reference Mission [4] available on:
http://caao.as.arizona.edu/PECO/PECO_DRM.pdf
- The PECO Technology Development Plan [5] available on:
http://caao.as.arizona.edu/PECO/PECO_techdev.pdf

The PIAA coronagraph requirements given in the next paragraph are derived from the PECO science requirements documents.

2.5. Coronagraph requirements for flight mission

Table 1 lists some of the key requirements for PECO. Our milestone will validate the requirements shown in green on the table. While the contrast and inner working angle requirements will be validated by laboratory measurements, the coronagraph concept throughput is a design parameter for the PIAA system, and does not need to be measured. The PIAA configuration adopted for our milestone offers a concept throughput (excluding losses due to optics coatings) higher than 80%.

PECO requires a contrast of 10^{-9} or better at $2 \lambda/D$ to bring residual starlight to a level comparable to or below the expected combined contribution of local zodiacal and exozodiacal light. If starlight exceeds 10^{-9} , the associated photon noise seriously reduces PECO's sensitivity and prevents imaging of most rocky planets. Imaging of giant planets is more tolerant to residual starlight and does not drive PECO's coronagraph performance requirements. Residual starlight needs to be calibrated to 10^{-11} or better to measure the planet's flux with a $\text{SNR}=10$ for a 10^{-10} contrast planet and accurately measure its position for orbit determination. This calibration can be achieved by relying on a combination of temporal (speckles originating from optical aberrations can be fixed in time and between targets), coherence (some residual speckles are coherent

with starlight) or spectral properties. We note that in PECO's technology development plan [5], the required raw contrast given in table 1 is 10^{-10} , while we aim in this milestone to demonstrate 10^{-9} contrast. The 10^{-9} raw contrast requirement is, as detailed above, fundamentally imposed by photon noise from the expected background level, but may not be sufficient if the residual light is poorly calibrated. In the more unfavorable case where all of the residual light is uncalibrated and cannot be distinguished from a true source through calibration or data processing, the raw contrast should be at 10^{-11} or better.

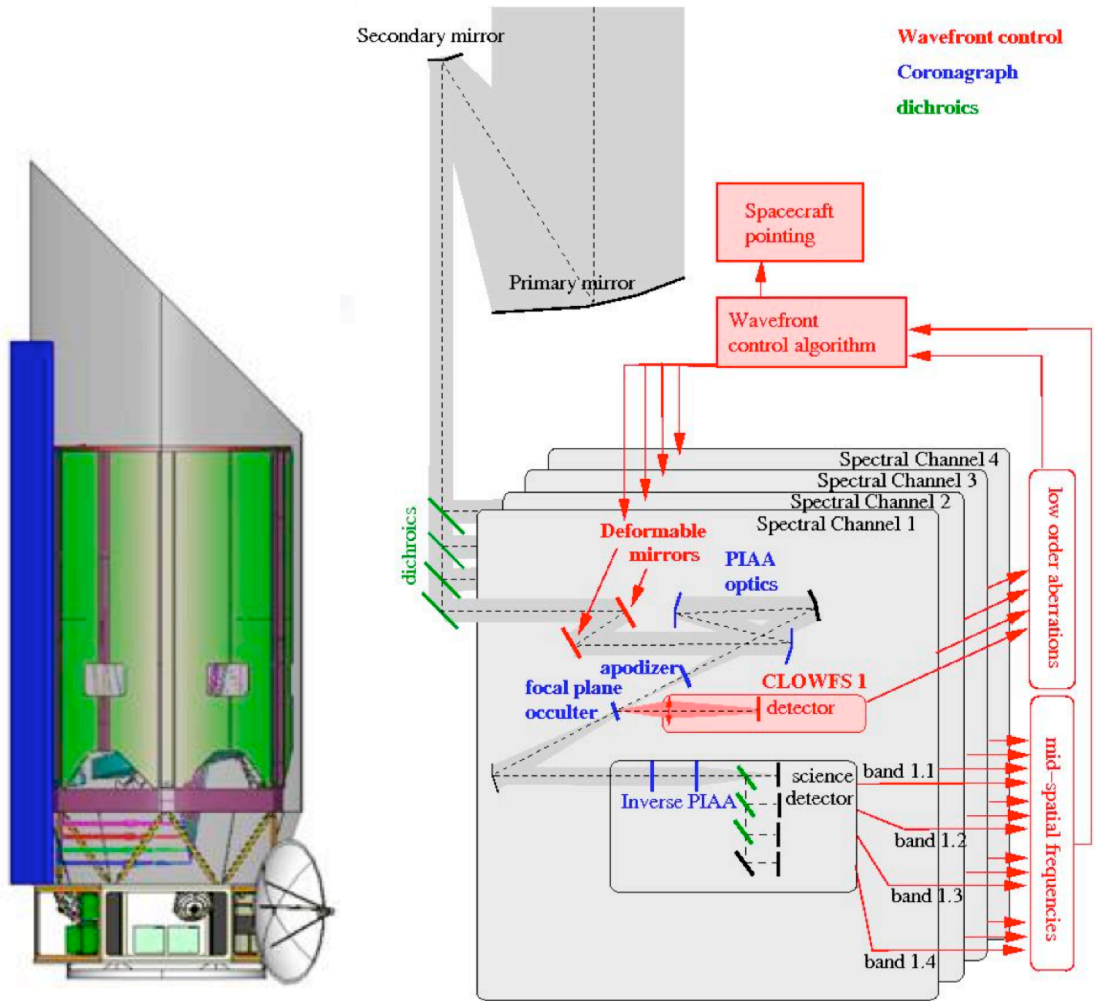


Figure 3: PECO spacecraft and optical telescope assembly

Figure 4: Baseline PECO coronagraph instrument architecture. Dichroics separate broadband (400nm - 900nm) light in 4 channels. Each channel includes its own PIAA coronagraph and wavefront control hardware, allowing all photons from 400nm to 900nm to be simultaneously used. Advances in polychromatic mask design and wavefront control may reduce the number of required channels.

Table 1: Main coronagraph requirements for the PECO mission for detection of terrestrial planets around 9 stars. Our milestone will validate requirements outlined in green in the table.

		Flight requirement for PECO	notes	Validation status and plan
1	Pointing (in coronagraph)	1 mas RMS jitter with 0.1 mas knowledge in bias variations	0.1 mas RMS jitter with < 0.1 mas knowledge demonstrated in air with PIAA [19]	Demonstrated on Subaru testbed. May also become future milestone for HCIT - see appendix B & C
2	Raw contrast level	must be below 10^{-09} if residual light is well understood and calibrated (note: PECO technology development plan document gives $1e-10$ requirement -see text for details)	equal to expected zodi + exozodi limit	Core objective of the milestone
3	Speckle contrast measurement precision	10^{-11}	Required to observe Earth-like planet	Future milestone - see appendix B
4	Coronagraph concept throughput: asymptotic value of throughput at large distance from the focal plane mask (excluding coating losses)	>80%	Subaru PIAA testbed using Axsys mirrors had 94.3% system throughput (excluding coating losses).	Enabled by PIAA design adopted for this milestone
5	Inner working angle (IWA)	#2 must be satisfied at $2 \lambda/D$, and coronagraph throughput at $2 \lambda/D$ should be 50% of system throughput at OWA		Enabled by PIAA design adopted for this milestone, see appendix A
6	Chromaticity	#2,#3,#4 and #5 must be met in >10% wide spectral band	Requires 2 DMs per channel. Goal is 20% wide band (PECO design)	Future milestone. Will require new optical layout and Tinsley PIAA optics - see appendix B
7	Outer working angle (OWA)	$16.5 \lambda/D$	function of the number of actuators across the pupil. Achieving $16.5 \lambda/D$ OWA requires an inverse-PIAA and more than 40 actuators across the pupil	Future milestone. Will require new optical layout. Low-contrast demonstration ongoing at Subaru (SCEXAO system) - see appendix A, B & D

These key performance metrics should be achieved in a 10 to 20% spectral band to avoid having to choose between a complex instrument design (too many spectral channels) and an inefficient observing sequence (scanning through spectral channels sequentially). The PECO baseline design uses 4 spectral channels, each 20% wide, to cover the 400 nm to 900 nm spectral range.

3. Milestone description: PIAA Monochromatic Contrast Demonstration

3.1. Milestone definition

“Demonstrate using Phase-Induced Amplitude Apodization a baseline contrast averaging 10^{-9} between a $2 \lambda/D$ inner working angle and a $4 \lambda/D$ outer working angle, in monochromatic light at a wavelength in the range of $400 \text{ nm} \leq \lambda \leq 900 \text{ nm}$.”

This milestone addresses several key aspects of the PECO performance error budget. PECO is required to form a high contrast “dark zone” over a working angle spanning $2 \lambda/D$ or less inner working angle to $15 \lambda/D$ outer working angle and a bandwidth of 400–900 nm. The HCIT testbed is addressing the most challenging location in the image plane, the inner working angle, at the same location required by PECO. The outer working angle for the flight mission is achieved using a large actuator count (at least 32×32 actuator for $15 \lambda/D$ outer working angle) deformable mirror (DM) located ahead of PIAA optics. The $2 \lambda/D$ out to $4 \lambda/D$ dark zone is of sufficiently large size that the physics of the wave front control problem can be demonstrated with high expectation of applying the same approach to a larger dark zone at a later date with a more capable optical design.

PECO must be capable of detecting light reflecting off of planets with intensity 10^{-10} fainter than that of the parent star. Ideally this is achieved by driving in the image the light surrounding the star to an intensity contrast ratio of residual light to parent starlight that is below 10^{-10} . However, the expected contrast from the exo-zodiacal light may reach 10^{-9} . In this milestone, we are required to demonstrate contrast reduction to the 10^{-9} raw contrast level. By achieving this result, we will have demonstrated image raw contrast performance that is limited not by the instrument but by the nature of the target.

Existing analytical and numerical models demonstrate that under ideal conditions contrasts are achievable at the performance level of the milestone. However, a complete error budget has yet to be validated with realistic error terms. While our milestone does not aim at developing such an error budget, this will be required for advancing the TRL for the PIAA mirrors as a component of a larger system. A complete error budget will require a thorough understanding of the environment provided by the HCIT (including wavefront stability in time and spatial coherence of the source).

3.2. Description of PIAA laboratory configuration

Optics

The completion of this first milestone is a direct continuation of ongoing work at HCIT and the Ames Coronagraph testbed. The optical configuration for the milestone will be identical to the current PIAA HCIT configuration (Figure 5). The same DM-after-PIAA arrangement is also currently used on the NASA Ames testbed.

Figure 5 shows the PIAA bench optical layout. The light source is located at the bottom right corner of the figure, and illuminates mirror PIAA M1 with a diverging spherical wave. Mirror PIAA M2 focuses the light to a first focal point, after which the beam is collimated by an off-axis parabola (OAP M3). A mild apodizer (opaque binary concentric rings pattern of metal deposited by microlithography on a clear glass substrate), designed to attenuate the faint edges of the PIAA-apodized beam, is located in this collimated space in a plane conjugated to PIAA M2. A second OAP (M4) then focuses the light to a second focus (F2), after which the diverging beam is recollimated by OAP M5. The DM is located in collimated space. OAP M7 focuses the beam on the focal plane mask (opaque disk of metal deposited by microlithography on a clear glass substrate), after which OAP M8 collimates the beam. Mirror M9 is a flat in collimated space, and OAP M10 focuses the light on the camera.

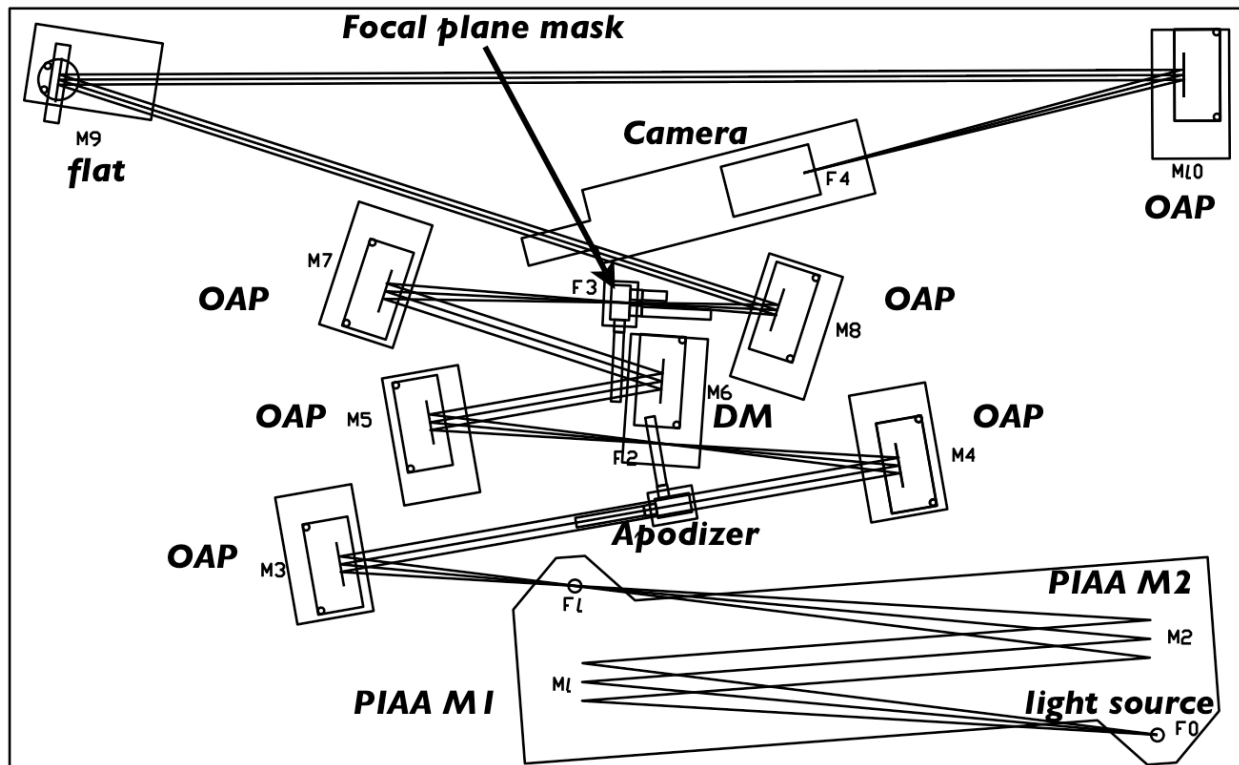


Figure 5: Optical layout of the PIAA testbed at HCIT. (Note: the Ames testbed optical layout is substantially different)

Wavefront control

Hardware: The wavefront is corrected by a single 32x32 actuator deformable mirror, located after the PIAA optics and before the focal plane mask. The mirror is manufactured by Xinetics and converts voltages into displacement of individual actuators bonded to a thin reflective mirror.

Wavefront measurement: The wavefront errors in the coronagraph are measured as a complex amplitude field in the focal plane of the camera. The steps to perform this measurement are as follows:

- (a) Acquire a focal plane image and measure the speckle field intensity in each pixel of the dark zone in the focal plane.
- (b) Compute a set of DM settings that will modulate the speckles in the dark zone by an amplitude comparable to their amplitude, and will produce sufficient diversity to solve for the coherent complex amplitude and incoherent light contribution on each pixel of the dark zone. The DM settings will therefore be a function of the speckle field intensity measured in (a), as there is a direct relationship between DM motion and amount of light introduced in the focal plane for the modulation. We note that several approaches are possible, for example, the algorithm currently used on HCIT aims at adding a nearly constant level of light over the dark zone, with this level adjusted to the mean speckle intensity in the dark zone. The algorithm previously in use at the Subaru testbed produced a modulation which matched for each pixel the intensity measured in (a).
- (c) Apply this sequence of DM settings and measure for each the resulting speckle field.
- (d) Using measurements obtained in (a) and (c), and the knowledge of the DM settings computed in (b), estimate, for each pixel of the dark field, the coherent and incoherent light contribution. Coherent light originates from residual wavefront errors, amplitude errors, and some coronagraph defects such as errors in the shape of the PIAA optics or apodizer. Incoherent light can be caused by ghosts, polarization effects, chromatic effects. Since the distinction between incoherent and coherent light is based on measuring if the light interferes with light added in the dark zone with the DM settings, we note that some coherent light may behave as incoherent light, and will therefore be considered incoherent in the experiment: coherent light that varies in phase or amplitude on timescales shorter than our measurement, or coherent light that varies in phase or amplitude within a single pixel of the detector.

Wavefront correction: Once the wavefront has been measured, a new DM setting is computed to minimize the coherent portion of the light in the dark field. The computation is based on inversion of the relationship between DM actuator displacements and complex amplitude in the dark zone. Variations on this scheme include Electric Field Conjugation (EFC) [25] and speckle nulling. We will employ wavefront control algorithms combined with human interaction to find a DM setting that achieves the 10^{-9} contrast.

3.3. Differences between Laboratory Demonstration and Flight

Environment

Our milestone will be achieved in a laboratory environment with a light source rather than the focal plane of a telescope at the input of the instrument. For the drift-away heliocentric orbit adopted for PECO, the thermal and vibration environment for the instrument will be more favor-

able in flight than in the laboratory. Stability issues can however be mitigated in the laboratory by increasing the source brightness to reduce the system response time.

Coronagraph system architecture

The coronagraph system architecture adopted for our milestone is simpler than for flight, as documented in Appendix A. We will use a single monochromatic coronagraph channel, while the flight instrument requires several polychromatic coronagraph channels to cover the full 400 nm to 900 nm spectral range.

An inverse PIAA is not required for this milestone, but will be required in the flight system to maximize the use of DM actuators and offer an outer working angle with a radius up to $0.5 \times N \lambda/D$, where N is the linear number of actuators across the beam. In this wide field architecture, the DM(s) need(s) to be located ahead of the PIAA optics. High contrast imaging of both sides of the focal plane requires two DM(s) to offer sufficient degrees of freedom.

Our milestone will adopt a simpler configuration with no inverse PIAA and only a single DM after the PIAA optics. This configuration will deliver a dark zone on one side of the focal plane only, and a small outer working angle ($4 \lambda/D$). The use of two DMs in the flight mission will yield the entire dark zone (both sides of the focal plane mask).

4. Computation of the Metric

4.1. Definitions

The contrast metric requires a measurement of the intensity of speckles appearing within the dark field, relative to the intensity of the incident star. The contrast metric will be assessed in terms of statistical confidence to capture the impact of experimental noise and uncertainties. In the following paragraphs we define the terms involved in this process, spell out the measurement steps, and specify the data products.

4.1.1. “Raw” Image and “Calibrated” Image. Standard techniques for the acquisition of camera images are used. We define a “raw” image to be the 2D array of pixel values image obtained by reading the charge from each pixel of the camera detector, amplifying and sending it to an analog-to-digital converter. We define a “calibrated” image to be a raw image that has had background bias subtracted and the detector responsivity normalized by dividing by a flat-field image. Saturated images are avoided by choosing appropriate settings for the exposure time, camera gain (if selectable) and source brightness in order to avoid the confusion of camera detector blooming and other potential camera detector nonlinearities. All raw images are permanently archived and available for later analysis.

4.1.2. We define “scratch” to be a DM setting in which actuators are set to a predetermined surface figure that is approximately flat (typically, about 20 volts on each actuator).

4.1.3. “Star”. We define the “star” to be a bare fiber tip, 0.22 numerical aperture with narrow-band light relayed via the optical fiber from a source outside the HCIT vacuum wall (e.g. 808 nm

frequency-stabilized laser). This “star” is the only source of light in the optical path of the HCIT. It is a stand-in for the star image that would have been formed by a telescope system.

4.1.4. "Wavefront control iteration". We define in this document "wavefront control iteration" to be a measurement of the complex amplitude in the dark zone followed by a DM correction aimed at removing coherent light in the dark zone, as detailed in section 3.2. Such iterations will be repeated for as many cycles as are needed to reach a desired level of speckle suppression.

4.1.5. The “Contrast field” is a dimension-less map representing for each pixel of the detector, the ratio of its value to the value of the peak of the central PSF that would be measured in the same conditions (camera setting, exposure time, central source illumination at the input of the instrument) if the coronagraph focal plane mask were removed. Measurement of the contrast field is detailed in sec. 4.4.

4.1.6. The “Contrast value” is a dimension-less quantity which is the average value of the contrast field over the dark zone adopted for the experiment. Its measurement is detailed in sec. 4.5.

4.1.7. “Statistical Confidence”. The interpretation of measured numerical contrast values shall take into consideration, in an appropriate way, the statistics of measurement, including for example speckle noise, detector read noise, photon counting noise, and dark-count noise.

The goal is to demonstrate with high confidence that the true contrast value (defined in sec 4.1.6.) is less than the required threshold contrast value C_θ . The estimated true contrast value shall be obtained from the average of a set of four or more contrast values measured in a continuous sequence (expected period of approximately one hour or more), each obtained with a new DM setting. For this milestone the required threshold is a mean contrast value of $C_\theta = 1.0 \times 10^{-9}$ with a confidence coefficient of 0.90 or better.

At any time in the demonstration, the HCIT contrast is subject to laboratory conditions, including the quality of the optical components, their alignment, any drift in their alignment over time, and the effectiveness of each wavefront sensing and control cycle. With each iteration, our nulling procedure attempts to improve the contrast metric, thus compensating for any drift or changes in alignment that may have occurred since the previous iteration, and variations may be expected due to experimental noise and any limitations in the algorithm. The distribution of contrast metrics for each iteration is regarded as random (Gaussian) about a mean contrast for the data set. We therefore consider the mean contrast as representative of the achieved contrast for a data set, and the distribution of contrast determinations among the DM settings for each set as a combination of both (random) speckle nulling variations and random measurement errors.

The mean contrast and confidence limits are computed in the following manner. The average of one or more images taken at each DM setting is used to compute the contrast metric. The mean contrast value for a set of images taken in a given hour is:

$$\hat{c} = \sum_{i=1}^n \frac{c_i}{n}$$

where n is the number of individual DM settings and images in each set and c_i is the contrast averaged over the dark zone for measurement i . The standard deviation σ each in the contrast values c_i obtained for individual DM settings within the set, which now includes both the meas-

urement noise and the (assumed random) contrast variations due to changes in the DM settings for each wavefront control iteration, is:

$$\sigma_{each} = \sqrt{\frac{\sum_{i=1}^n (c_i - \hat{c})^2}{n-1}}$$

Our estimate \hat{c} is subject to uncertainty in the contrast measurements $\sigma_{mean} = \sigma_{each} / \sqrt{n}$ and the independently-determined overall errors in photometry σ_{phot} . We will assume gaussian statistics about the mean contrast to derive a statistical confidence. Then the statistical confidence that the mean contrast is less than $C_0 = 1 \times 10^{-9}$ is given by:

$$conf = \frac{1}{\sqrt{2\pi}} \int_{-\infty}^t e^{-z^2/2} dz$$

where $t = (C_0 - \hat{c}) / \sigma$ and $\sigma = \sqrt{\sigma_{mean}^2 + \sigma_{phot}^2}$. The values \hat{c} and σ are the milestone metrics. The 90% confidence contrast value is thus the value C_0 such that $conf(C_0) = 0.9$ according to the above equations. Although we assume a gaussian statistics for the contrast values to compute the 90% confidence contrast, we will make the full set of measurement available to enable independent analysts to compute the 90% confidence interval for other statistics. One data product will be a goodness of fit of the measurement with a normal distribution (Kolmogorov-Smirnov test).

Speckle statistics behind coronagraphs is described by Soummer et al 2007 [26] to obey a Rician distribution, which is noticeably different from the gaussian statistics we assume to compute the confidence interval of our measurement. In the HCIT PIAA experiment, the speckle temporal distribution at any given location in the focal plane is unlikely to be an offset gaussian, and we note that it is also unlikely to be Rician. The Rician statistics describe the speckle statistics only if their complex amplitude can be written as the coherent sum of a static component and a dynamic component with a 2-D gaussian distribution. We do not expect that these assumptions will be valid on a space coronagraph, or in our experiment, for several reasons:

- We expect some level of incoherent light due to ghosts, polarization issues and chromatic issues (this last issue is not applicable to our milestone). In current HCIT measurements, our speckles are dominated by an incoherent component which has not been well characterized and could be variable in time.
- The coronagraph is an active system where speckles are used to sense optical aberrations. Weak coherent speckles will be poorly measured as they may be lost in the photon noise and incoherent background, while brighter speckles will be better measured. With a gaussian distribution of wavefront errors at the input of the system, the expected output is therefore expected to be flatter than a gaussian.
- Unlike atmospheric turbulence, the temporal behavior of wavefront errors in HCIT is not accurately described as a gaussian. We expect a large contribution from slow drifts. With a non-predictive controller, a slow drift will produce a nearly static coherent residual. We would

then expect many long-lived slow complex amplitude speckles instead of a 2-D gaussian temporal distribution.

Given the current uncertainties in the temporal behavior of the wavefront disturbances in the HCIT, the unknown behavior of incoherent light and the currently unknown degree of predictive control to be introduced in the loop, we cannot anticipate with confidence what the statistical temporal distribution of single speckle intensities will be.

Our proposed analysis on the confidence interval is however using the averaged contrast over the dark zone, which is an average of approximately 100 independent diffraction limited domains (we note that speckles in the PIAA system are linearly 3 times smaller than the telescope diffraction limit on the sky, due to remapping), each with its own speckle statistics (Gaussian, Rician or other). Photon noise and readout noise will also add to the true speckle noise. Through the combination of this spatial averaging and the different sources of noise we expect, a statistical distribution of the contrast values close to a gaussian is a reasonable assumption (central limit theorem). This assumed gaussian distribution will only be used to derive a confidence interval, but we will also deliver the full set of measurements which can be used to test, through a Kolmogorov-Smirnov test, statistical confidence that the values obtained obey a gaussian distribution (or any other distribution).

4.2. Measurement of the Star Brightness

The brightness of the star is required to compute contrast, and is measured with the following steps.

- 4.2.1. The occulting mask is laterally offset by at least $10 \lambda/D$, so as to eliminate the effect of the occulting mask at the location of the star image.
- 4.2.2. A deep non-saturated image of the star is taken by adding many frames, with all coronagraph optics other than the focal plane mask in place (PIAA optics, binary apodizer, focal plane mask substrate).
- 4.2.3. In this deep image, the peak intensity is related to some average over a part of the PSF that is not covered up by the occulter and is not much affected by the DM (far out in the DM transfer function).
- 4.2.4. This ratio is then applied to any subsequent measurement of the speckle field, by multiplying the image by a constant to produce speckle intensities on a relative scale where the star image would have a peak value of unity.

4.3. Measurement of the focal plane scale

In the PIAA system configuration adopted for our first milestone, there are no inverse-PIAA optics, and the off-axis PSF is therefore highly distorted. As a result, the focal plane scale (camera pixels per λ/D) estimation cannot use the translation invariance of the PSF. The following definition will be adopted;

The focal plane scale is defined by the displacement (pixels) of the PSF’s photocenter in the absence of a focal plane mask in the system for a physical displacement of the light source by $f\lambda/D$, where f and D are respectively the focal length and diameter of beam at the input of the system (before PIAA optics).

All angular separations given in this document adopt this definition. The PSF photocenter is defined as the intensity-weighted center of the PSF, and it is a linear function of the source position at the input of the system: with the above definition, the focal plane scale value obtained is independent of the source offset used in the measurement. We will empirically measure the focal plane scale by moving the light source by a known amplitude and measuring its photocenter, and verify that the obtained scale matches the value expected from the optical design of the PIAA mirrors and re-imaging optics.

4.4. Measurement of the Coronagraph Contrast Field

Each “coronagraph contrast field” is obtained as follows:

4.4.1. The occulting mask is placed on the star image.

4.4.2. A long-exposure (e.g. seconds) image is taken of the coronagraph field (i.e. the suppressed star plus surrounding speckle field) with the coronagraph focal plane mask in place. The dimensions of the dark zone target areas are defined as follows: A dark zone extending from 2 to $4\lambda/D$, demonstrating a useful search space, is bounded by a line that passes $2\lambda/D$ from the star

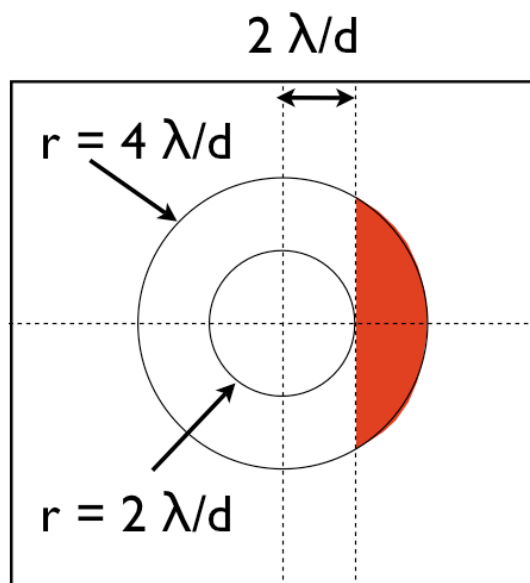


Figure 6: Dark zone geometry. The high contrast region is shown in red.

at its closest point, and by a circle of radius $4\lambda/D$ centered on the star (see Figure 6).

4.4.3. The resulting image is divided by the peak value of the reference star to produce a “contrast field” image, as discussed in Sec. 4.2.

4.5. Contrast value for a single measurement

The contrast field (sec 4.4.) is averaged within the dark zone (Figure 6) to yield the contrast value for a single measurement. This averaging is done over a single image (which itself may consist of a co-addition of consecutive camera frames) with no statistical filtering other than removal of detector defects (bad pixels, cosmic rays). The D shape of the dark zone covers an area equal to $9.8(\lambda/D)^2$ on the sky, so the contrast value is an average of ~ 100 diffraction-limited speckles (speckles in the PIAA system are linearly 3 times smaller than λ/D on the sky, due to the re-mapping). The dark zone area which is inside $3\lambda/D$ of the optical axis is $3.47(\lambda/D)^2$. We note that a contrast value equal to 10^{-9} does therefore not ensure that the contrast at $2\lambda/D$ is equal to

10^{-9} : it could be obtained with a 2.8×10^{-9} average contrast from 2 to $3 \lambda/D$ and no light (infinite contrast) from 3 to $4 \lambda/D$.

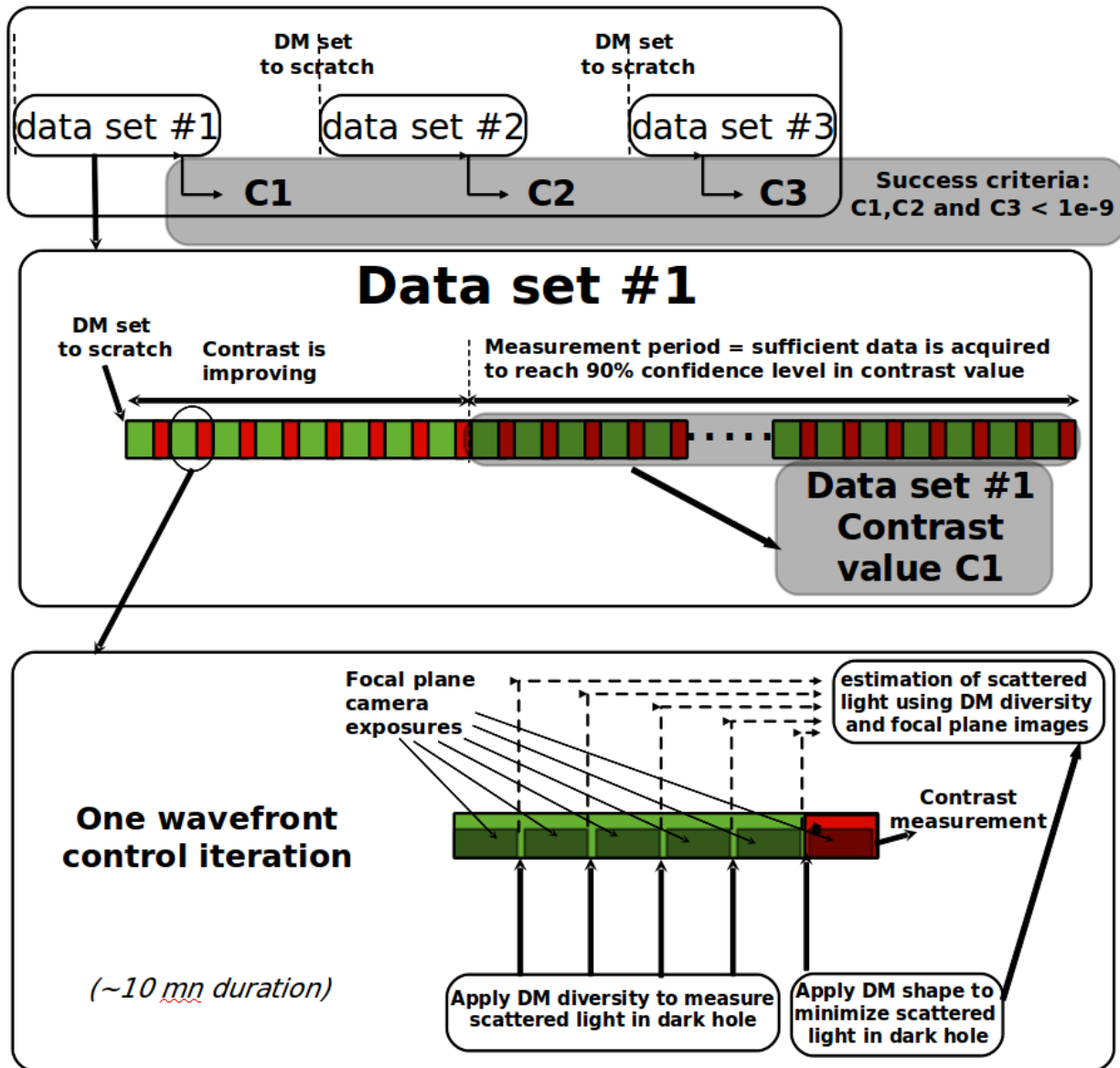


Figure 7: Data acquisition sequence. The success criteria is met when three data sets each meet the 10^{-9} contrast criteria. Data acquisition is detailed for one set in the central part of the figure. A set consists of a succession of wavefront control iterations and contrast measurements. One such wavefront control iteration is shown in the lower part of the figure.

4.6. Milestone Validation Demonstration Procedure

The Milestone validation demonstration procedure, shown in Figure 7, is as follows:

4.6.1. The DM is set to scratch with a reset of the wavefront control system software.

4.6.2. Wavefront control iterations (sec 4.1.4) are performed to iteratively converge to settings of the DM actuator driver voltages that give an acceptable high-contrast wavefront solution for the target dark zone. This typically takes from one to several hours, starting from scratch, if no prior information is available.

4.6.3. When contrast in the dark zone stops improving, the high-contrast measurement begins while the wavefront control iterations are being performed, as described below:

- Wavefront control iterations are continuously performed at a speed which optimizes contrast in the target dark zone (typically one wavefront control iteration every few minutes).

- As described in Sec. 4.1.4(a), for each wavefront control iteration, one measurement is acquired with the best DM shape for high-contrast (no additional deformation on the DM to probe speckles). This measurement is used toward contrast measurement, and is referred to as the contrast field image.

4.6.4. Contrast field images are acquired by repeating step 4.6.3. The contrast metric is measured for each of the contrast field images on each pixel within the dark zone.

4.6.5. The following images are to be archived for future reference: raw and calibrated coronagraphic images, all DM voltage commands, coronagraph transmittance profile

4.6.6. The following images or data are to be presented in a final report:

- calibrated images of the reference star,

- the coronagraph transmittance profile and focal plane scale

- a set of contrast field images

- a contrast metric value for the target area in each of the contrast field images

- a statistical analysis of the contrast values, with the 90% confidence contrast value for the data set

- a histogram of the brightness distribution of pixels in the dark field for each of the high contrast images in the data set, and for the combined data acquired in each data set.

5. Success Criteria

The following are the required elements of the milestone demonstration. Each element includes a brief rationale.

5.1. Illumination is monochromatic light in single or dual polarization at a wavelength in the range of $400 \text{ nm} < \lambda < 900 \text{ nm}$.

Rationale: *This milestone is a monochromatic experiment to demonstrate feasibility of the approach at a wavelength in the science band of PECO.*

5.2. A mean contrast metric of 1×10^{-9} or smaller shall be achieved in a 2 to 4 λ/D dark zone, as defined in Sec. 4.4.

Rationale: *This provides evidence that the high contrast field is sufficiently dark (10^{-9} expected exozodi level) to be useful for searching planets, and test whether there is a fundamental limitation at the inner working angle.*

5.3. Criterion 5.2, averaged over the data set, shall be met with a confidence of 90% or better, as defined in Sec. 4.1.5. Sufficient data must be taken to justify this statistical confidence.

Rationale: *Assuming the contrast values have a Gaussian distribution about the mean contrast, this demonstrates a statistical confidence of 90% that the mean contrast goal has been reached.*

5.4. Elements 5.1 – 5.3 must be satisfied on three separate occasions with a reset of the wavefront control system software (DM set to scratch) between each demonstration.

Rationale: *This provides evidence of the repeatability of the contrast demonstration.* The wavefront control system software reset between data sets ensures that the three data sets can be considered as independent and do not represent an unusually good configuration that cannot be reproduced. For each demonstration the DM will begin from a "scratch" setting and the algorithm used to converge will have no memory of settings used for prior demonstrations. There is no time requirement for the demonstrations, other than the time required to meet the statistics stipulated in the success criteria. There is no required interval between demonstrations; subsequent demonstrations can begin as soon as prior demonstrations have ended. There is also no requirement to turn off power, open the vacuum tank, or delete data relevant for the calibration of the DM influence function.

6. Certification Process

The Principal Investigator will assemble a milestone certification data package for review by the Exoplanet Exploration Program and its Technology Advisory Committee. In the event of a consensus determination that the success criteria have been met, the Program will submit the findings of the TAC, together with the certification data package, to NASA HQ for official certification of milestone compliance. In the event of a disagreement between the Program and the TAC, NASA HQ will determine whether to accept the data package and certify compliance or request additional work.

6.1 Milestone Certification Data Package

The milestone certification data package will contain the following explanations, charts, and data products.

- 6.1.1. A narrative report, including a discussion of how each element of the milestone was met, an explanation of each image or group of images, appropriate tables and summary charts, and a narrative summary of the overall milestone achievement.
- 6.1.2. Calibrated images of the coronagraph transmittance profile.
- 6.1.3. Calibrated images of the 3 sets of data, with appropriate numerical or color-coded or grey-scale coded contrast values indicated, and with coordinate scales indicated in units of Airy distance (λ/D), all in demonstration of achieving the milestone elements.
- 6.1.4. A histogram of the brightness distribution of pixels in the dark field for each of the high contrast images in the data set, and for the combined data acquired in each data set.
- 6.1.5. A set of contrast measurement values for each of the 3 data sets
- 6.1.6. A description of the residual components of the residual light in the dark zone: static coherent light, dynamic coherent light (due to time-variable pointing errors and wavefront changes too rapid to be fully corrected by the wavefront control loop) and incoherent light (ghosts, polarization leaks).
- 6.1.7. A step by step description of all data processing and analysis performed, along with source code and algorithm description. This will be provided in sufficient detail so an independent analysis of the raw data can be applied outside our team

7. References

- [1] PECO website: <http://caao.as.arizona.edu/PECO>
- [2] PECO report to astro2010: http://caao.as.arizona.edu/PECO/PECO_Report.pdf
- [3] PECO science requirements document: http://caao.as.arizona.edu/PECO/PECO_SRD.pdf
- [4] PECO design reference mission: http://caao.as.arizona.edu/PECO/PECO_DRM.pdf
- [5] PECO Technology Development Plan: http://caao.as.arizona.edu/PECO/PECO_techdev.pdf
- [6] Guyon, O. "Phase-induced amplitude apodization of telescope pupils for extrasolar terrestrial planet imaging," A&A, v.404, p.379-387 (2003)
- [7] "[Two-Mirror Apodization for High-Contrast Imaging](#)" Traub, Wesley A.; Vanderbei, Robert J. ApJ, 599, 695 (2003)
- [8] "[Pupil Mapping in Two Dimensions for High-Contrast Imaging](#)" Vanderbei, Robert J.; Traub, Wesley A. ApJ, 626, 1079 (2005)
- [9] "Exoplanet Imaging with a Phase-induced Amplitude Apodization Coronagraph. I. Principle" Guyon, O., Pluzhnik, E.A., Galicher, R., Martinache, F., Ridgway, S.T., Woodruff, R.A., ApJ, 622, 744-758 (2005)

- [10] "Exoplanet Imaging with a Phase-Induced Amplitude Apodization Coronagraph. II. Performance", Martinache, F., Guyon, O., Pluzhnik, E.A., Galicher, R., Ridgway, S.T., ApJ, 639, 1129-1137, (2006)
- [11] "[Diffraction Analysis of Two-dimensional Pupil Mapping for High-Contrast Imaging](#)" Vanderbei, Robert J. ApJ, 636, 528 (2006)
- [12] "Exoplanet Imaging with a Phase-Induced Amplitude Apodization Coronagraph. III. Diffraction Effects and Coronagraph Design", Pluzhnik, E.A., Guyon, O., Ridgway, S.T., Martinache, F., Woodruff, R.A., Blain, C., Galicher, R., ApJ, 644, 1246-1257, (2006)
- [13] Guyon, O., Pluzhnik, E.A., Kuchner, M.J., Collins, B., Ridgway, S.T., "Theoretical Limits on Extrasolar Terrestrial Planet Detection with Coronagraphs", ApJ Suppl, 167, 81 (2006)
- [14] Lozi, J., Martinache, F., Guyon, O. "Phase-Induced Amplitude Apodization on centrally obscured pupils: design and first laboratory demonstration for the Subaru Telescope pupil", PASP, Volume 121, Issue 885, pp. 1232-1244 (2009)
- [15] "High Performance PIAA Coronagraphy with Complex Amplitude Focal Plane Masks", submitted, http://www.naoj.org/staff/guyon/publications/2009-10_PIAACMC.pdf
- [16] EXCEDE http://nicmosis.as.arizona.edu:8000/POSTERS/AAS_EXCEDE_04JAN08C.pdf
- [17] Levine, M. et al., "Levine, M., et. al (2009) Terrestrial Planet Finder – Coronagraph (TPF-C) Flight Baseline Mission Concept", white paper provided to the 2010 Decadal Survey (2009)
- [18] Guyon, O.; Pluzhnik, E.A.; Martinache, F; Totems, J.; Tanaka, S.; Matsuo, T.; Blain, C.; Belikov, R. "High Contrast Imaging and Wavefront Control with a PIAA Coronagraph: Laboratory System Validation", PASP (2010), http://www.naoj.org/staff/guyon/publications/2009-11-07_PIAA_labexp.pdf
- [19] Guyon, O., Matsuo, T., Angel, R., "Coronagraphic Low Order Wavefront Sensor: Principle and Application to a Phase-Induced Amplitude Coronagraph", ApJ, 693, pp 75-84 (2009)
- [20] Belikov, Ruslan; Pluzhnik, Eugene; Connelley, Michael S.; Witteborn, Fred C.; Lynch, Dana H.; Cahoy, Kerri L.; Guyon, Olivier; Greene, Thomas P.; McKelvey, Mark E., SPIE, Volume 7440, pp. 74400J-74400J-12 (2009)
- [21] Kern et al., "Phase-induced amplitude apodization (PIAA) coronagraph testing at the High Contrast Imaging Testbed", Techniques and Instrumentation for Detection of Exoplanets IV. Edited by Shaklan, Stuart B. Proceedings of the SPIE, Volume 7440 (2009)
- [22] Phase-induced amplitude apodization M1 mirror re-figuring, <http://prod.nais.nasa.gov/cgi-bin/eps/synopsis.cgi?acqid=136681>
- [23] Breckinridge, James B.; Oppenheimer, Ben R., "Polarization Effects in Reflecting Coronagraphs for White-Light Applications in Astronomy", ApJ, 600, 1091 (2004)
- [24] Balasubramanian, Kunjithapatham; Hoppe, Daniel J.; Mouroulis, Pantazis Z.; Marchen, Luis F.; Shaklan, Stuart B. "Polarization compensating protective coatings for TPF-Coronagraph optics to control contrast degrading cross polarization leakage", Proc. SPIE, 5905 (2005)

- [25] Give'on, Amir; Kern, Brian; Shaklan, Stuart; Moody, Dwight C.; Pueyo, Laurent, "Broad-band wavefront correction algorithm for high-contrast imaging systems" Proc. SPIE, 6691 (2007)
- [26] Soummer, Rémi; Ferrari, André; Aime, Claude; Jolissaint, Laurent "Speckle Noise and Dynamic Range in Coronagraphic Images", ApJ, Vol 669, pp. 642-656

Appendix A: PIAA coronagraph architecture

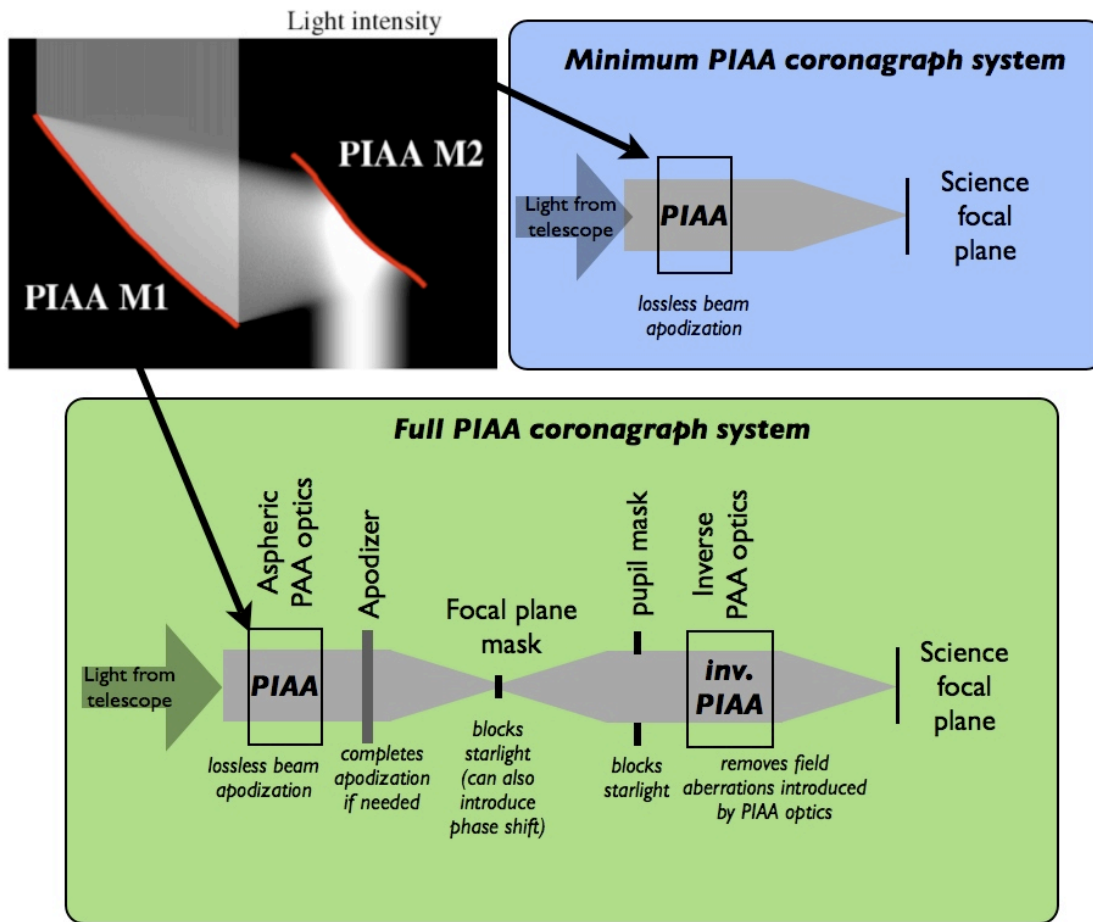


Figure A-1: Two example of PIAA coronagraph system architectures. Both architectures use a set of aspheric optics (top left) to perform lossless apodization of the telescope beam. The minimum PIAA coronagraph system (top right) consists of a PIAA apodization unit introduced before the instrument's focal plane detector array. A full PIAA coronagraph system (bottom) can also include an apodizer, a focal plane mask, a pupil stop and an inverse PIAA optics unit.

There are several possible coronagraph architectures using PIAA optics. Figure A-1 shows both the minimum PIAA coronagraph conceptual architecture, and a full architecture. The minimum architecture simply produces an image after the PIAA optics. The central source's light is highly concentrated in a single narrow diffraction spot, allowing much fainter off-axis sources to be imaged. This simple architecture, which is described in Guyon et al 2003 [6], is however limited in both performance and manufacturability :

- The PIAA optics are very difficult to manufacture when designed for high contrast. In this PIAA design, the outer edge of the first PIAA mirror is highly curved. This feature, which is essential for obtaining the desired apodization, is extremely difficult to polish.
- Chromatic diffractive propagation of the wavefront at the edge of the beam prevents high contrast in broadband light. This effect was first identified in Vanderbei 2005 [11]

- The off-axis image quality is poor, as first shown in [Guyon 2003 \[6\]](#)
- This configuration, as shown in Figure 1, does not have a focal plane mask and requires the camera detector to record a high contrast image.

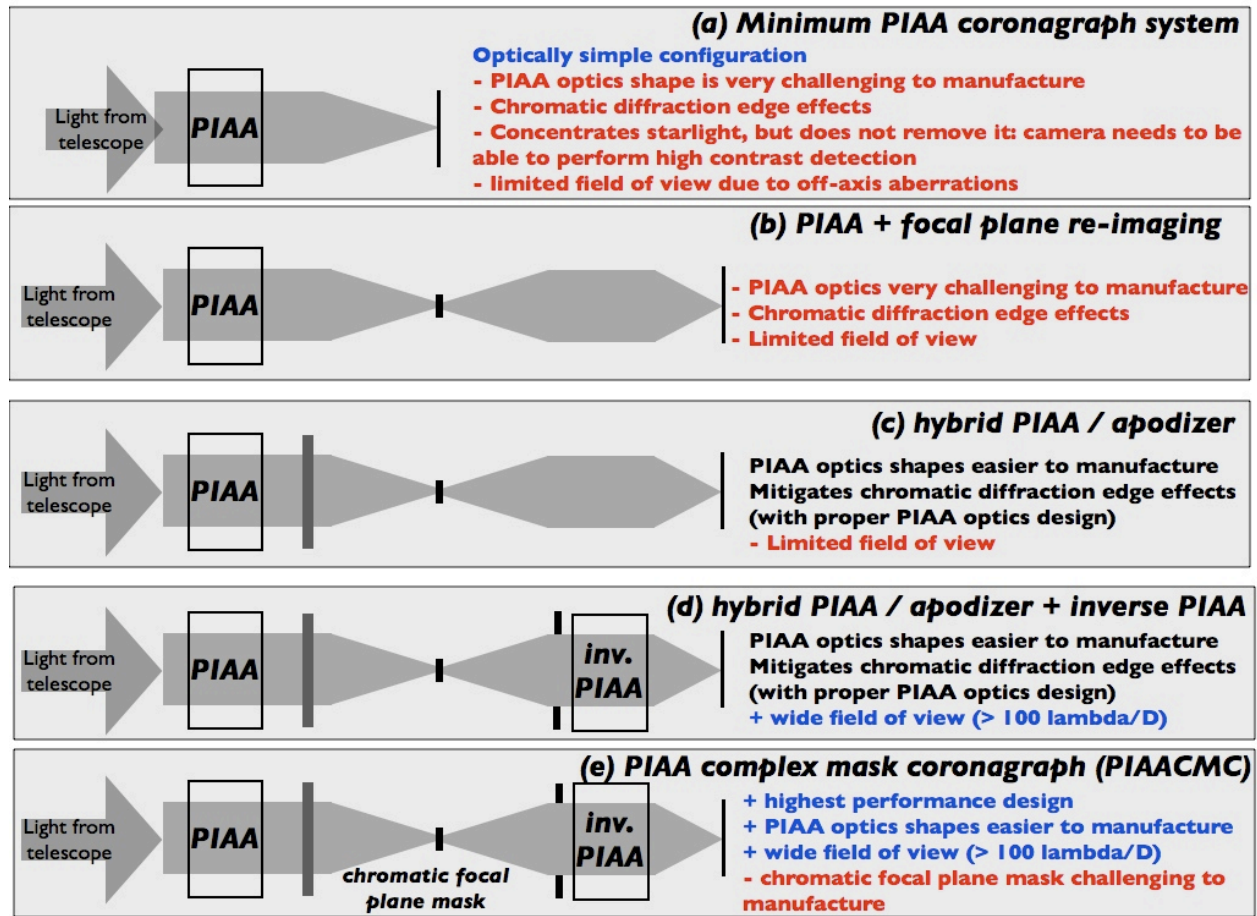


Figure A-2: Five possible PIAA coronagraph architectures, approximately ordered from top to bottom in increasing performance and manufacturing ease. For milestone 1, architecture (c) is adopted

These issues can be solved or mitigated with a more complete PIAA system design, as shown in the bottom of Figure A-1. A complete PIAA system includes the following components in addition to the PIAA aspheric optics:

- A focal plane mask followed by optics to re-image the focal plane on the science detector. The focal plane mask removes the light from the central star and does not require any optical component or detector located downstream of the mask to support high contrast imaging
- An apodizer located after the PIAA optics, but before the focal plane mask. The role of the apodizer is to share the apodization with the PIAA optics. This allows re-design of the PIAA optics to greatly improve manufacturability and reduce the chromatic propagation effects at the edge of the beam. These gains are documented in [Pluzhnik et al. 2006 \[12\]](#)

- A pupil mask (Lyot mask) located after the focal plane mask. This pupil mask allows the PIAA coronagraph to be designed as an Apodized Pupil Lyot Coronagraph which achieves starlight suppression with both the focal plane mask and the Lyot mask, and offers superior performance
- A set of inverse PIAA optics to recover a diffraction limited PSF over a wide field of view. This set of optics, first suggested in [Guyon 2003 \[6\]](#), was demonstrated in the laboratory by [Lozi et al. 2009 \[14\]](#)
- A complex amplitude focal plane mask to compensate for the chromatic change in PSF size at the focal plane.

Figure A-2 shows five possible PIAA system configuration implementing none (a), a subset (b-d) or all (e) of the components listed above. The HCIT PIAA milestone 1 experiment will adopt architecture (c).

Figure A-3 shows how these architectures compare in both performance and technical difficulty (mostly manufacturing). The manufacturing challenges associated with each of the five architectures are listed in the table shown on Figure A-4. New PIAA concepts allow increased performance while making the PIAA aspheric optics easier to manufacture. For example, the PIAA optics in the recently developed PIAACMC concept [15] are easier to manufacture than the PIAA optics currently used in the HCIT, although this concept requires a transmissive phase-shifting focal plane mask to be manufactured.

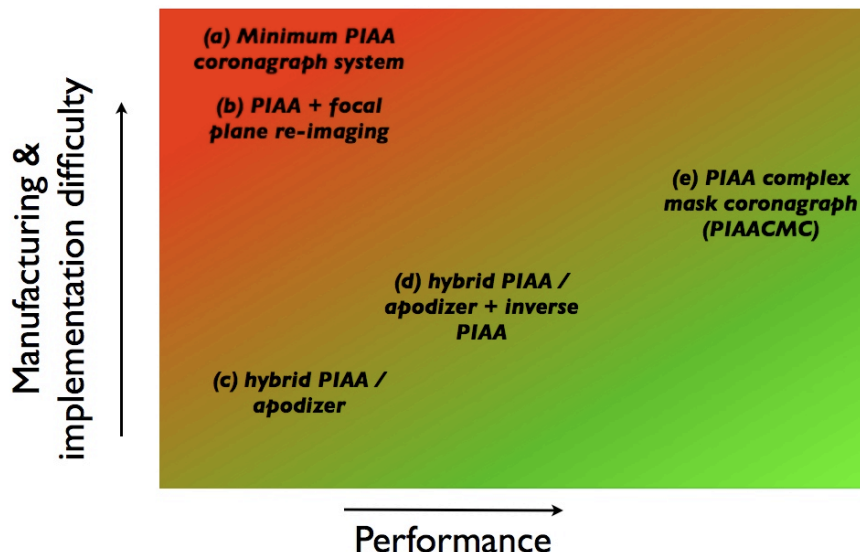


Figure A-3: Approximate location of the five architectures shown in Figure 2 on a 2-D plane with performance (x axis) and degree of technical difficulty (y axis) coordinates.

Manufacturing challenges

Coronagraph component	(a) Minimum PIAA coronagraph system or (b) PIAA + focal plane re-imaging	(c) PIAA/Apodizer hybrid	(d) PIAA/Apodizer hybrid + inverse PIAA	(e) PIAACMC	Notes
PIAA optics	Extreme asphericity, strong chromatic propagation effects	Challenging aspheric optics manufacturing		Milder apodization reduces aspheric departure	PIAA optics asphericity can be traded against apodizer strength
Apodizer	No apodizer required	Apodizer only affects edges of the beam		No apodizer required	Stronger apodizer = lower system throughput
Focal plane mask	Fully opaque	Fully opaque	Fully opaque	Slightly transmissive, phase shifting with chromatic dependence	
Inverse PIAA	No inverse PIAA	Can be refractive or reflective Needs to be diffraction-limited			Inverse PIAA needs to be diffraction-limited and can be smaller and of lower optical quality than direct PIAA

Figure A-4: For each of the four architectures, manufacturing challenges are different, as shown in this table.

Wavefront control in a PIAA system: importance of deformable mirror location

In a PIAA system, the relationship between DM actuator number and dark zone size is non-intuitive. In the configuration adopted for milestone 1, a 32x32 DM gives us a $4 \lambda/D$ outer working angle. In the configuration proposed for milestone 2 in the PIAA TDEM proposal, the same DM sampling gives us an outer working angle of $15 \lambda/D$. This issue has always been quite confusing as it is very specific to PIAA systems and is tied to the location of the DM(s) in the PIAA system.

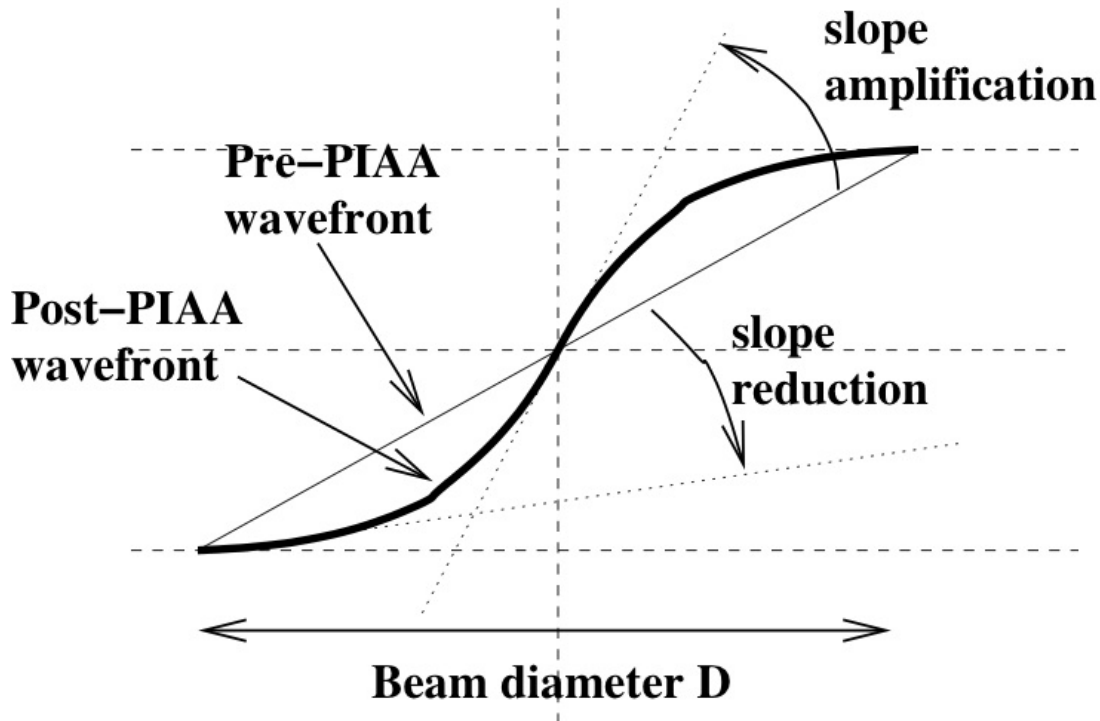


Figure A-5: Slope amplification and reduction factors in a PIAA system. The remapping introduced by a PIAA system amplifies the wavefront slope at the center of the apodized beam (where most of the light is located) and reduces the wavefront slope at the edges of the beam

The outer working angle (OWA) is defined by the furthest (from the optical axis) speckles that the DM(s) can cancel in the science focal plane. In non-PIAA coronagraph and with actuators organized on a regular square grid, the OWA is therefore $(N/2) \times (\lambda/D)$, where N is the number of actuators along the diameter of the pupil. The OWA then appears in high contrast adaptive optics (AO) systems as the size of the "high contrast" box in the focal plane. In a PIAA system this straightforward relationship becomes more complicated, due to the pupil remapping. The location of the deformable mirror in a PIAA system can therefore have a large impact on the outer working angle (OWA) of the system. Because of the remapping, the local radial slope of the wavefront finds itself magnified by the local value of the apodization function [10]. If one notes $A(r)$ the radial apodization profile after PIAA remapping (in square root of the intensity), the

post-PIAA wavefront radial slope of an off-axis source (angular separation α , azimuth θ_0) therefore writes as:

$$\delta\varphi(r,\theta)/\delta r = \alpha A(r) \cos(\theta-\theta_0).$$

The Figure A-5 illustrates the impact of the remapping on the wavefront slope: in the inner part of the beam, where $A(r)$ is maximum, the slope is amplified by a factor $\beta_a > 1$, while near the outer edge of the beam, it is reduced by a factor $\beta_r < 1$. Typical values for these factors are $\beta_a = 3$ and $\beta_r = 0.3$. Because in the post-PIAA beam, most of the light is concentrated toward the center of the beam. It is therefore this part of the wavefront, and the factor β_a that will define the location of the off-axis image pseudo-core.

These factors can quantitatively be used to estimate the OWA for several PIAA+DM system configurations (Figure A-6), in which the DM(s) must correct for wavefront errors both before and after the remapping :

- Configuration 1 (DM located after the PIAA optics, no inverse PIAA). The angular distance α of each off-axis source perceived by the deformable mirror is amplified by β_a . The OWA of this configuration is therefore reduced by the same amount, that is $(N/2)/\beta_a$ elements of resolution. Beyond this separation, the DM does not have sufficient actuator density at the center of the pupil: if the actuators were mapped to the entrance of the PIAA, they would be too large at the center of the beam.
- Configuration 2 (DM located before the PIAA optics, no inverse PIAA). If the actuators were mapped to the output of the PIAA, we find that the actuator size at the edge of the apodized beam is divided by $\beta_r < 1$ (the actuators are bigger), while they are considerably smaller in the center of the apodized beam. In the outer part of the beam, the DM sampling can only allow full control of speckles to radius $r = \beta_r \times (N/2) \times (\lambda/D)$, corresponding to $OWA = (\beta_r / \beta_a) \times (N/2) \times (\lambda/D)$ on the sky. We note that a larger OWA can be reached if speckles are only corrected over a fraction of the field, and the the OWA limits given in this section only apply to a half field dark zone for a single DM correction or a full field dark zone for a dual DM correction.

In both configurations 1 and 2, the unaberrated field of view is limited to $r \sim 5 \lambda/D$ by the field aberrations introduced by the PIAA optics. This effect is described in Figures 4 to 7 in Guyon et al. 2005 [9]. There is therefore little advantage to increasing the wavefront control OWA much beyond this radius, although it can be beneficial to do so in polychromatic light to avoid chromatic speckles within the OWA due to non-linear frequency folding of speckles just outside the OWA (Guyon 2005 [25]). We note that the OWA and the unaberrated field of view are equal for $N \sim 30$ and $N \sim 100$ in configurations 1 and 2 respectively. We now explore configurations including inverse PIAA optics to provide a wide unaberrated field of view ($> 100 \lambda/D$ in radius as shown in Guyon et al 2005 [9], Figure 11). In these configurations, the field of view for high contrast observations is limited by the OWA of the wavefront control system.

- Configuration 3 (DM ahead of PIAA optics). In this configuration, the inverse PIAA cancels the effect of the forward PIAA, and the OWA is equal to what it would be

in a non-remapped system: $OWA = (N/2) \times (\lambda/D)$. The only role of the remapping is to create an intermediate step where starlight is efficiently removed by the focal plane mask.

- Configuration 4 (DM after PIAA optics). The OWA can be found by remapping the DM geometry in the plane ahead of the forward PIAA, where its actuators will be magnified by β_a at the center of the pupil. The OWA, defined by the largest actuator in this plane, is therefore $OWA = (1/\beta_a) \times (N/2) \times (\lambda/D)$.

In order to optimize the use of a given number of actuators, the DM(s) should therefore be placed after the PIAA optics in a PIAA system without inverse PIAA optics (configuration 1), or before the PIAA optics if inverse PIAA optics are included (configuration 3). The configuration adopted in our laboratory demonstration is configuration 1 (DM after PIAA optics, no inverse PIAA optics).

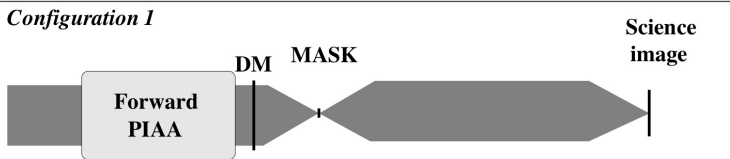
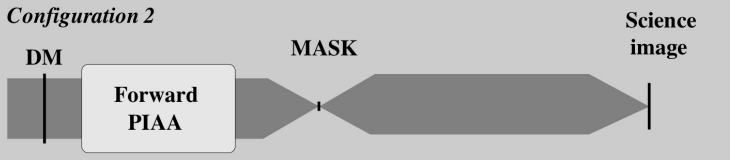
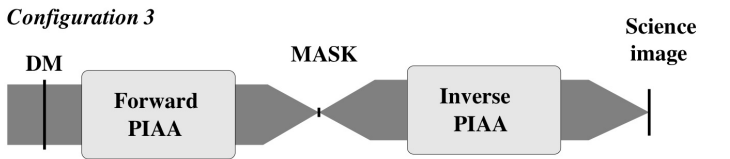
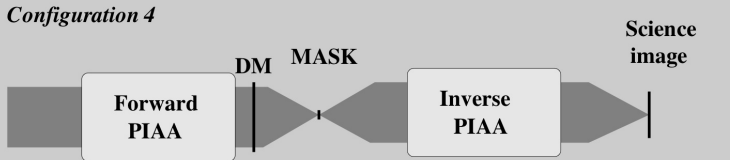
		Wavefront Control Outer Working Angle (OWA)	Unaberrated Field of View
<i>Configuration 1</i>		$OWA = (1/3) \times (N/2) \times (\lambda/D)$	$\sim 5 \lambda/D$
<i>Configuration 2</i>		$OWA = 0.1 \times (N/2) \times (\lambda/D)$	$\sim 5 \lambda/D$
<i>Configuration 3</i>		$OWA = 1.0 \times (N/2) \times (\lambda/D)$	$> 100 \lambda/D$
<i>Configuration 4</i>		$OWA = (1/3) \times (N/2) \times (\lambda/D)$	$> 100 \lambda/D$

Figure A-6: Four possible architectures for a PIAA coronagraph with wavefront control. For each configuration, the outer working angle of the wavefront control system and the field of view imposed by remapping are given. The PIAA slope amplification factor $\beta_a = 3$ and slope reduction factor $\beta_r = 0.3$ are considered here. Configurations shown in gray (configurations 2 and 4) should be avoided (see text for details). The unaberrated FOV values are given assuming $N=32$ actuators across the pupil diameter.

Appendix B: Possible future milestones and relationship between testbeds

Future milestones expected to follow the monochromatic starlight suppression milestone are briefly described in this appendix. Our work plan is making use of previous work and the Ames testbed to prepare these milestones for HCIT.

Pointing control and low order wavefront sensor

With a 1 mas RMS pointing control at the coronagraph focal plane mask, pointing-induced coronagraphic leaks reach 10^{-9} contrast at $2 \lambda/D$ in PECO, and brings as much photon noise as the expected zodi+exozodi floor. Pointing errors must therefore be smaller than 1 mas RMS on PECO. In addition to this photon noise imposed requirement, pointing-induced light must be calibrated to 10^{-11} contrast level to allow SNR=10 measurement of 10^{-10} contrast sources, corresponding to a 0.1 mas knowledge or stability of the pointing zero point (average pointing position during the observation of a single target).

While a 0.1 mas PECO-equivalent pointing control was demonstrated at the Subaru Telescope PIAA testbed with a low order wavefront sensor, this testbed has been discontinued, and we plan to repeat this measurement on a testbed reaching 10^{-9} contrast. More details on the PECO pointing requirements and pointing control strategy are given in Appendix C.

High contrast in polychromatic light

PECO requires a 10^{-9} contrast in a 10% broad spectral band (goal = 20% broad spectral band for full efficiency observations with 4 coronagraphic channels). A future milestone will be written based on this requirement.

Residual light calibration to 10^{-11} contrast level

While there is little gain in pushing the contrast below 10^{-9} since the combined zodi and exozodi levels are expected at 10^{-9} contrast, potentially habitable planets will be at $\sim 10^{-10}$ contrast. SNR=10 observations of such sources therefore requires calibration of the components of residual starlight at the 10^{-11} contrast level. A future milestone will be written based on this requirement.

Demonstration of Outer Working Angle (OWA)

The outer working angle is the largest angular separation at which high contrast observations can be made. In a high contrast system, it is limited in part by the number of actuators N across the DM, as actuator sampling in the pupil dictates the focal plane separation from the optical axis within which speckles can be controlled:

$$\text{OWA} = [\lambda/D] \times (N/2)$$

In a PIAA system, reaching this OWA requires the use of inverse PIAA optics, which undo the pupil mapping introduced by the PIAA optics. The inverse PIAA optics are located at the back end of the coronagraph, after starlight has been removed, and serve two purposes:

- they ensure optimal use of DM actuators for the coronagraph OWA. Without inverse PIAA, the OWA equation above cannot be met.
- they remove strong off-axis aberrations introduced with the PIAA optics. These aberrations would otherwise limit the useful field of view to approximately $5 \lambda/D$, regardless of DM actuator count

In a future milestone, we plan to demonstrate $15 \lambda/D$ OWA with a 32×32 actuator DM on HCIT. The Subaru Telescope SCExAO system and the Ames testbed will perform wavefront control to $15 \lambda/D$ OWA with a 32×32 actuator DM prior to HCIT, ensuring that vacuum time is used efficiently for this milestone. A detailed description of inverse PIAA optics is given in Appendix D.

Appendix C: Pointing control

Requirements for PECO

- (1) The telescope pointing should be stable within 10 mas on hour timescales. This requirement is imposed by beam walk on optics, which, if pointing is not stable, will create speckles as pointing changes.
- (2) The instrument pointing tolerance during observations is no more than 1% of the diffraction width (i.e. <math><1\text{ mas}</math>) to keep the pointing contribution to raw contrast at or below 10^{-9} . This first requirement is imposed by photon noise sensitivity.
- (3) In addition to the pointing jitter requirement described above, the time-averaged position of the star image over the focal plane coronagraph mask should be stable (or known) to within 0.1mas over a period of a few hours to avoid coherent mixing of starlight leaks with residual speckles. This second requirement is imposed by calibration issues: detection of planets at the IWA of the coronagraph can easily be confused by small pointing offsets.

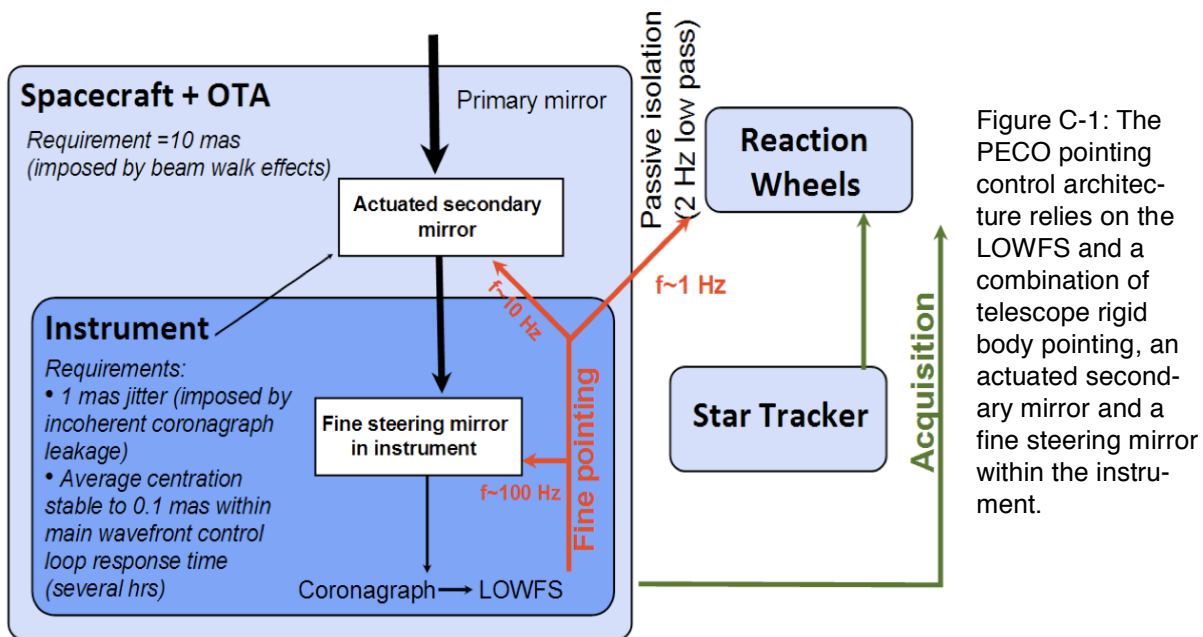


Figure C-1: The PECO pointing control architecture relies on the LOWFS and a combination of telescope rigid body pointing, an actuated secondary mirror and a fine steering mirror within the instrument.

Pointing control strategy on PECO

The PECO strategy to meet this stability is fourfold:

- 1) Operate in a very stable environment far from Earth (heliocentric orbit)
- 2) Eliminate vibration coupling from the reaction wheels by using a hexapod isolation system under each reaction wheel and design the OTA and optical mounting for stiffness
- 3) Derive an accurate control signal from the bright target star image reflected by the coronagraphic stop. The LOWFS measures sub-mas pointing errors at $>100\text{ Hz}$.
- 4) Use the actuated telescope secondary mirror (momentum compensated) and fine steering the DMs conjugated to the pupil within the instrument to meet the tight instrument pointing tolerance (1 mas) with a relaxed OTA pointing requirement of 10 mas. Using HST as a bench-mark

(<10 mas pointing stability in LEO), our models show we will meet the OTA pointing requirement.

Low Order Wavefront Sensor (LOWFS) demonstration with PIAA coronagraph system

The low order wavefront sensor concept and implementation are described in [19]. We summarize here results obtained with the LOWFS on the Subaru PIAA system and discuss their relevance to both the HCIT PIAA experiment and the PECO pointing control strategy described above.

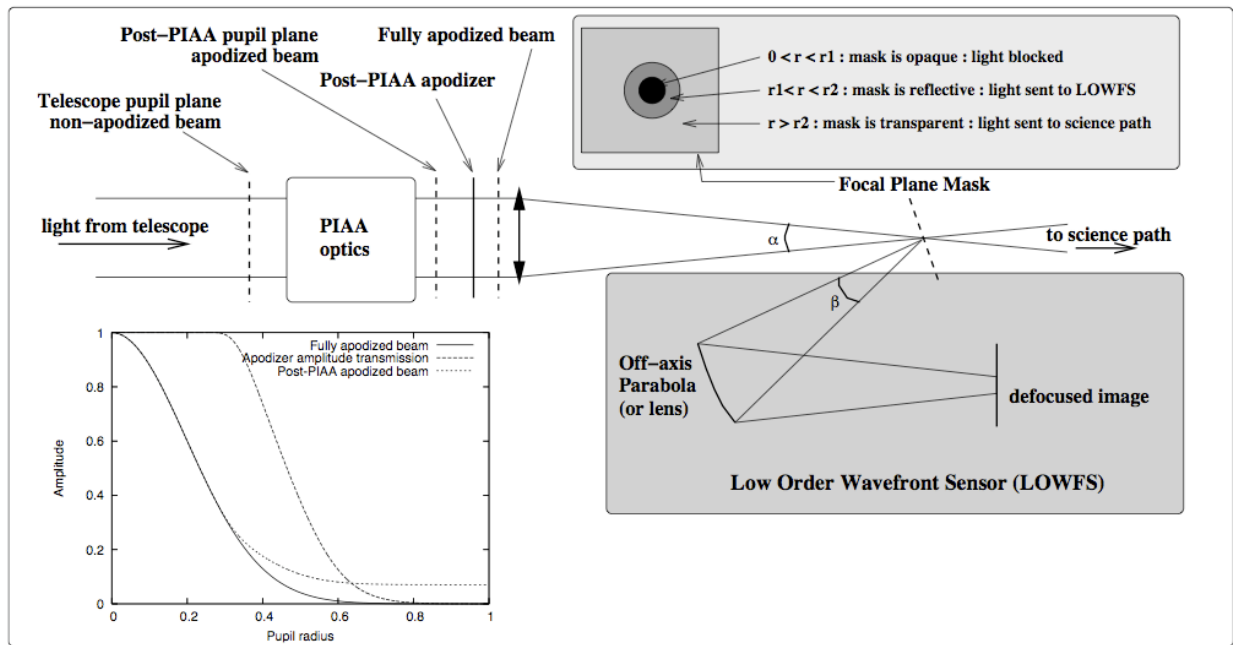


Figure C-2: LOWFS architecture. A dual zone focal plane mask extracts starlight from the focal plane to measure pointing.

LOWFS: principle

As shown in Figure C-2, the LOWFS uses starlight falling on the coronagraph focal plane mask: this light would otherwise be lost by the coronagraph. Thanks to a focal plane mask with a dark central zone surrounded by a reflective annulus, the LOWFS is insensitive to non-common path errors and does not require exquisite calibration of its detector. The large amount of incident light on the focal plane mask allows fast (>100 Hz) and accurate (<mas) unbiased measurement of pointing.

Results obtained in LOWFS prototype at the Subaru testbed - relevance to HCIT and PECO

Results obtained on the Subaru testbed with a LOWFS operating in visible light are summarized in Figure C-3, taken from [19]. The experiment was performed in air on a testbed which is not as stable as HCIT (or PECO). As shown in the lower left panel of Figure C-3, the source stability over 1-hr is approximately $0.01 \lambda/D$ RMS (1 mas on PECO). After closed loop correction, the source is maintained to about $0.001 \lambda/D$ RMS (0.1 mas on PECO) jitter with <0.1 mas drift over one hour, which exceeds the PECO flight requirement.

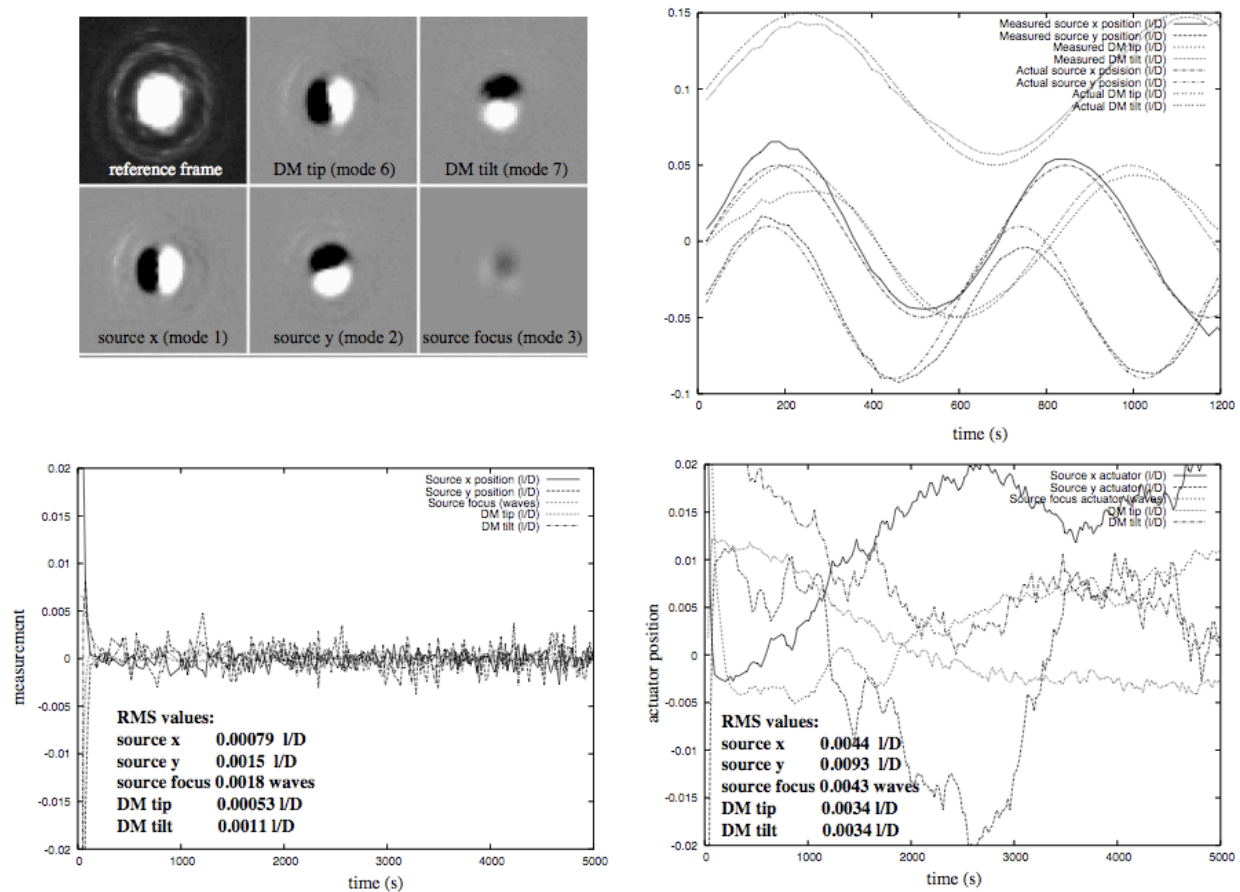


Figure C-3: Laboratory performance for the CLOWFS. Upper left: Measured CLOWFS reference frame and influence functions for the 5 axis controlled in the experiment. Pre-PIAA and post-PIAA modes look extremely similar, as expected. Top right: Open loop simultaneous measurement of pre and post-PIAA modes. The measured amplitudes match very well the sine-wave signals sent to the actuators, and the CLOWFS is able to accurately measure all 4 modes shown here with little cross-talk. Since this measurement was performed in open loop, the measurement also includes unknown drifts due to the limited stability of the testbed. Bottom left: Closed loop measurement of the residual error for the 5 modes controlled. The achieved pointing stability is about $10^{-3} \lambda/D$ for both the pre-PIAA and post-PIAA tip/tilt. Bottom right: Position of the actuators during the same closed loop test.

Appendix D: Inverse PIAA optics

←

The inverse PIAA optics role is to remove the strong off-axis aberrations introduced by the PIAA optics. After the PIAA optics, the image of off-axis sources becomes strongly aberrated; the inverse PIAA optics are designed to re-concentrate light of these sources in a Airy-like pattern with good translation-invariance.

Off-axis aberrations in a PIAA system

Off-axis aberrations due to the beam shaping performed by the PIAA optics are very strong (Figure D-1), but also well understood. Optics can therefore be designed to remove these aberrations.

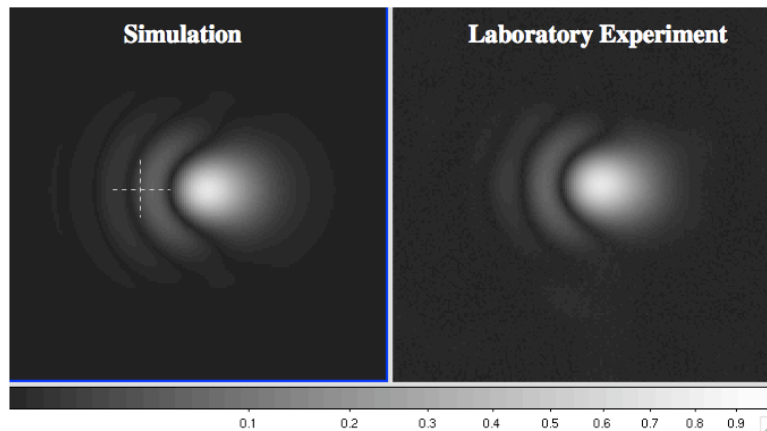


Figure D-1: Simulated vs. actual off-axis PSF in the Subaru PIAA testbed. The match between the two PSFs is excellent, illustrating that off-axis aberrations in the PIAA system are well understood. Similar results have been obtained on the HCIT and Ames PIAA systems.

Design of inverse PIAA

Optics: Inverse-PIAA optics are designed exactly like PIAA optics. They are simply mounted backward to perform the inverse remapping of the PIAA optics. Since the inverse PIAA optics are located after the focal plane mask (and Lyot mask if there is one), they do not need to be coronagraphic quality (they must be however be diffraction limited). This allows considerable flexibility in the design of the inverse PIAA optics:

- inverse PIAA optics can be physically much smaller than direct PIAA optics, thanks to relaxed optical quality requirements and negligible impact of Fresnel diffraction effects due to their small size
- inverse PIAA optics can be refractive, as moderate chromatic aberrations are allowed as long as diffraction limit is maintained

System design: The location of the inverse PIAA along the beam needs to be chosen properly to minimize beam-walk effects between the PIAA and inverse PIAA. If the inverse PIAA is too far in conjugation space from the direct PIAA, light from an off-axis source will not travel through the same part of the inverse PIAA as it did through the PIAA, which can limit the field of view. With proper placement of the inverse PIAA, the corrected diffraction limited field of view can reach $100 \lambda/D$ in radius.

Simulated performance

A detailed analysis of the inverse PIAA optics performance is given in reference [9]. While in principle the inverse PIAA perfectly reverses the remapping introduced by the PIAA, this approximation is valid only when the off-axis PSF is unaffected by the focal plane mask and is sufficiently close to the optical axis for beam walk effect to be small:

- close to the optical axis, the focal plane mask removes part of the off-axis PSF, leading to a change in PSF flux and shape in the final focal plane after the inverse PIAA optics (Figure D-2)
- far from the optical axis, beam walk effect introduce second-order amplitude and phase effects in the output pupil of the inverse PIAA (Figure D-3).

Simulations in Figures D-2 and D-3 however indicate that the PSF is very close to an Airy function in the dark zone of a PECO-like mission (2 to 16 λ/D).

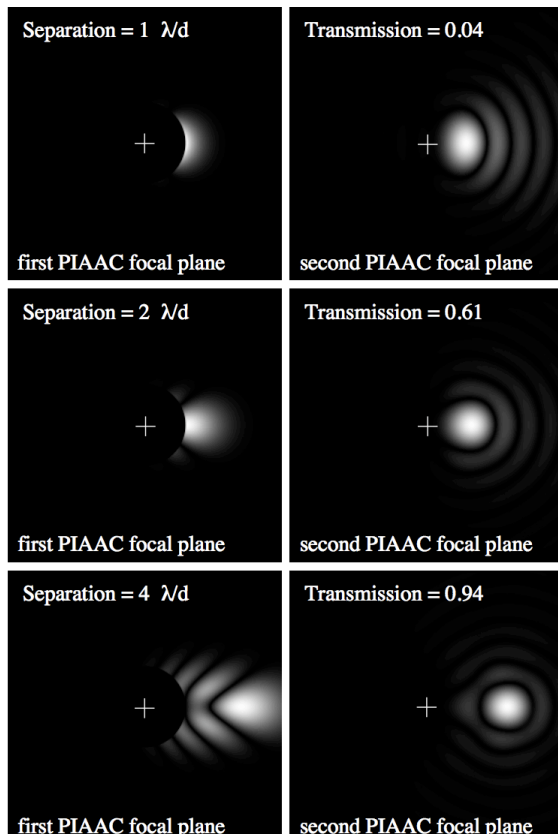


Figure D-2: Simulated PSFs in the intermediate (left) coronagraph focal plane, immediately after the focal plane mask, and the final (right) focal plane after the inverse PIAA.

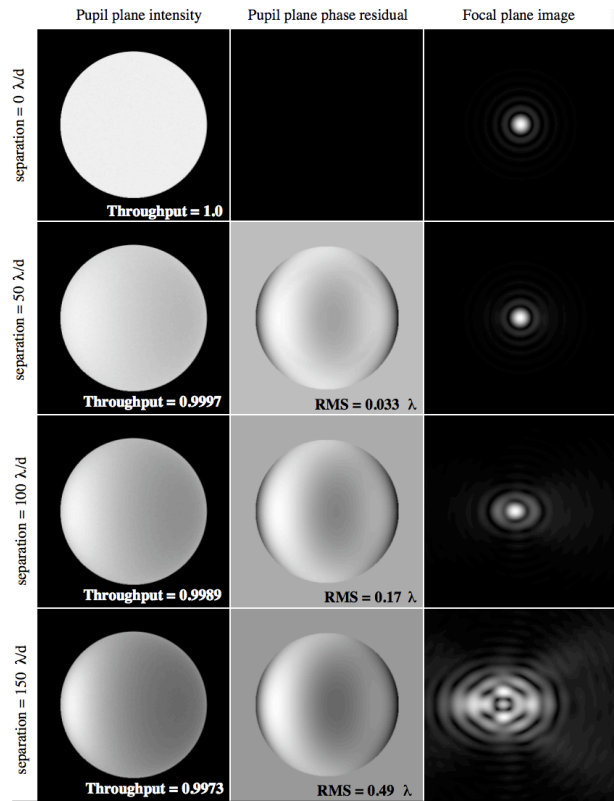
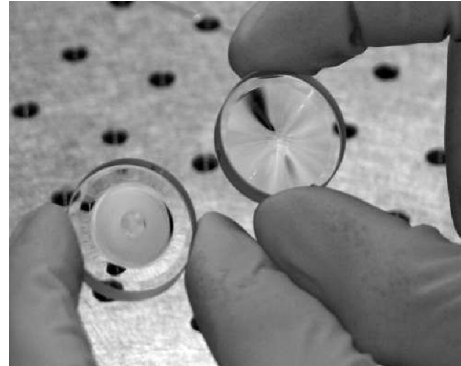


Figure D-3: With properly placed inverse PIAA optics, the diffraction-limited field of view can reach 100 λ/D in radius (simulations).

Demonstration of field correction with inverse PIAA optics at Subaru Telescope

The Subaru Coronagraphic Extreme-AO (SCEXAO) system includes a PIAA coronagraph with both direct and inverse PIAA, in a DM-ahead of PIAA configuration. SCEXAO's inverse PIAA unit is of direct relevance to PECO, and serves as a demonstration of the inverse PIAA technique.

The first prototype of SCEXAO's inverse PIAA optics consisted of 25 mm diameter lenses (16 mm beam size) separated by 96 mm (see Figure D-4). A smaller set of inverse PIAA lenses in a very compact configuration (8 mm diameter beam, 48 mm spacing between the lenses) is now in use on SCEXAO. With such small lenses, diamond turning can yield high quality diffraction-limited imaging with no need for testing and post-polishing. The lenses are therefore inexpensive and can be made rapidly. The SCEXAO inverse PIAA lenses were made by Axsys imaging technologies.



The beam shaping performed by the SCEXAO PIAA optics is more extreme than for the PIAA HCIT experiment or PECO: the SCEXAO PIAA system simultaneously apodizes the beam and removes the telescope large central obstruction. This results in very strong off-axis aberrations. Figure D-5 (taken from [14]) shows these aberrations (second line), and shows that the inverse PIAA removes them very efficiently. This test, performed without wavefront control, shows that a diffraction-limited image can be produced over the full high contrast field, and that chromatic effects are sufficiently mild with small refractive optics (the test was performed in the visible with optics designed for 1.6 μm wavelength).

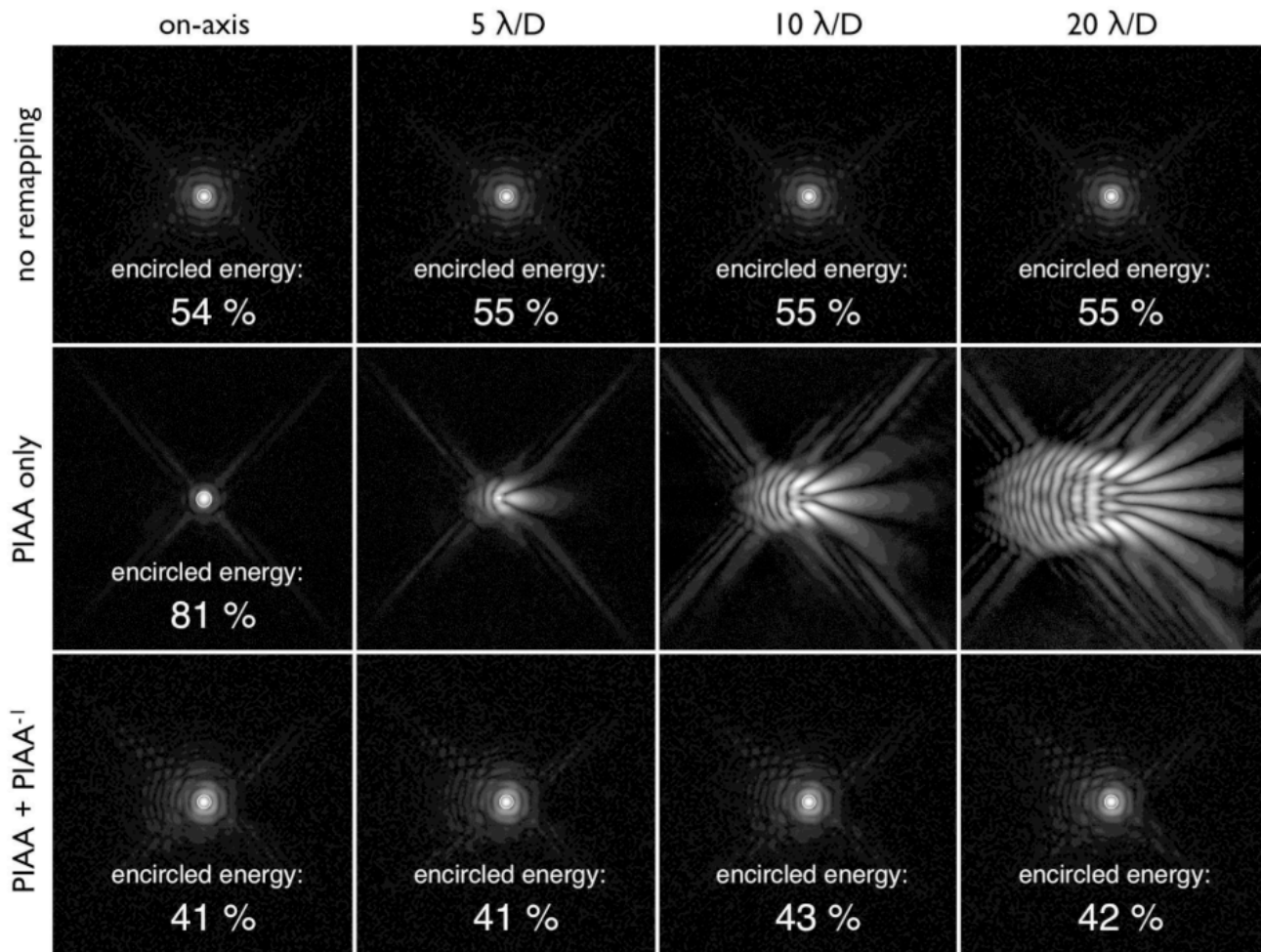


Figure D-5: Inverse PIAA demonstration on the SCEXAO system. The images after PIAA (middle row) show large off-axis aberrations which are well corrected by inserting the inverse PIAA optics (lower row).